

# JGR Earth Surface

## RESEARCH ARTICLE

10.1029/2023JF007326

### Key Points:

- WaterGAP3 water model data overestimate daily runoff variability in snowmelt-influenced watersheds
- Global relationships between mean runoff and daily runoff variability are strongly mediated by snowmelt fraction
- Topographic drivers of mean runoff, snowmelt fraction, and daily runoff variability are best assessed at the mountain range scale

### Supporting Information:

Supporting Information may be found in the online version of this article.

### Correspondence to:

A. M. Forte,  
aforte8@lsu.edu

### Citation:

Forte, A. M., & Rossi, M. W. (2024). Stochastic in space and time: 1. Characterizing orographic gradients in mean runoff and daily runoff variability. *Journal of Geophysical Research: Earth Surface*, 129, e2023JF007326. <https://doi.org/10.1029/2023JF007326>

Received 4 JUL 2023

Accepted 8 JAN 2024

### Author Contributions:

**Conceptualization:** A. M. Forte, M. W. Rossi  
**Data curation:** A. M. Forte  
**Formal analysis:** A. M. Forte, M. W. Rossi  
**Investigation:** A. M. Forte, M. W. Rossi  
**Methodology:** A. M. Forte  
**Resources:** M. W. Rossi  
**Visualization:** A. M. Forte  
**Writing – original draft:** A. M. Forte  
**Writing – review & editing:** A. M. Forte, M. W. Rossi

## Stochastic in Space and Time: 1. Characterizing Orographic Gradients in Mean Runoff and Daily Runoff Variability

A. M. Forte<sup>1</sup>  and M. W. Rossi<sup>2</sup> 

<sup>1</sup>Department of Geology and Geophysics, Louisiana State University, Baton Rouge, LA, USA, <sup>2</sup>Earth Lab, Cooperative Institute for Research in Environmental Sciences (CIRES), University of Colorado, Boulder, CO, USA

**Abstract** Mountain topography alters the phase, amount, and spatial distribution of precipitation. Past efforts focused on how orographic precipitation can alter spatial patterns in mean runoff, with less emphasis on how time-varying runoff statistics may also vary with topography. Given the importance of the magnitude and frequency of runoff events to fluvial erosion, we evaluated whether orographic patterns in mean runoff and daily runoff variability can be constrained using the global WaterGAP3 water model data. Model runoff data are validated against observational data in the contiguous United States, showing agreement with mean runoff in all settings and daily runoff variability in settings where rainfall-runoff predominates. In snowmelt-influenced settings, runoff variability is overestimated by the water model data. Cognizant of these limitations, we use the water model data to develop relationships between mean runoff and daily runoff variability and how these are mediated by snowmelt fraction in mountain topography globally. A global analysis of topographic controls on hydroclimatic variables using a random forest model was ambiguous. Instead, relationships between topography and runoff parameters are better assessed at the mountain range scale. Rulesets linking topography to mean runoff and snowmelt fraction are developed for three mid-latitude mountain landscapes—British Columbia, European Alps, and Greater Caucasus. Increasing topographic elevation and relief together leads to higher mean runoff and lower runoff variability due to the increasing contribution of snowmelt. The three sets of empirical relationships developed here serve as the basis for a suite of numerical experiments in our companion manuscript (Part 2, Forte & Rossi, 2024a, <https://doi.org/10.1002/2023JF007327>).

**Plain Language Summary** It has long been understood that mountain ranges can have profound influences on the location and intensity of precipitation, for example, through the formation of rain shadows. Less clear is how these “orographic effects” are reflected in the details of river runoff, specifically how much runoff varies from day-to-day. Understanding this variability of runoff is important as differences in variability directly influence how rivers respond to changes in rock uplift rate. Here, we use results from a global water model integrated with topography data to explore how runoff variability is related to topography in high relief landscapes. Consistent with prior work, we find and expand on the observation that mean runoff and runoff variability are inversely correlated and that the nature of their relation fundamentally depends on how much runoff comes from snowmelt as opposed to rain. In turn, both mean runoff and the importance of snowmelt are positively correlated with aspects of topography. Our results imply that incorporating variability into models of coupled developing orographic patterns in runoff and landscape evolution is critical and we identify a simple framework within which to develop such models. Examples of these models are presented in a companion work (Part 2, Forte & Rossi, 2024a, <https://doi.org/10.1002/2023JF007327>).

## 1. Introduction

Weather systems develop over the course of hours to weeks depending on their size (e.g., Trenberth et al., 2003), while landscapes evolve over millennia and longer. Climatic drivers of the long-term evolution of mountain belts (Whipple, 2009) are impeded by this mismatch in timescale. Modeling weather and hydrology over long timescales is a substantial computational challenge (e.g., Shen et al., 2021), and thus the choices made in the representation of the hydroclimate are often baked into the simplified process laws we use to construct landscape evolution models. For fluvial landscapes, the most widely used model for river incision and relief development is the stream power model (Howard, 1994; Whipple & Tucker, 1999). The details of this model have been expounded elsewhere (e.g., see reviews in Kirby & Whipple, 2012; Lague, 2014; Whipple & Tucker, 1999; Whipple et al., 2022; Whittaker, 2012) and we present a more complete synopsis in Part 2 (Forte & Rossi, 2024a).

In short, the shear stress formulation of stream power asserts that fluvial erosion can be expressed as the product of three terms: a coefficient describing the efficiency of erosion, drainage area raised to an exponent, and local slope raised to another exponent. The latter two terms and the ratio of the exponents can be constrained using topographic data alone (e.g., Wobus et al., 2006), leaving the coefficient of erosion and the value of the slope exponent to account for a large number of important process parameters including climate. While unpacking the assumptions underlying generalized forms of stream power have been addressed by many papers (e.g., Kirby & Whipple, 2012; Lague, 2014; Whipple et al., 2022), we highlight two sets of assumptions of stream power that motivate our analysis of global runoff data. First, it is common to use a drainage area as a proxy for discharge. Orographic precipitation (Galewsky, 2009; Roe, 2005) is mimicked in 1D stream power models by adding additional area dependence on runoff that alters concavity (Roe et al., 2002) and fluvial relief (Roe et al., 2003). In 2D, these basic effects tend to be more ambiguous (Han et al., 2014) and produce discordance between mainstem and tributary morphology (Leonard & Whipple, 2021). Second, simple stream power typically assumes a characteristic discharge, thus entailing either that erosion thresholds are negligible or that the effects of thresholds are subsumed within the stream power parameters itself. This latter possibility has now been carefully examined by changing the temporal scale over which river erosion is modeled (i.e., at the daily scale). By integrating stream power over the probability distribution of flows above erosional thresholds (Lague et al., 2005; Snyder et al., 2003; Tucker, 2004; Tucker & Bras, 2000), the response of river profiles to climate is not only embedded in the coefficient of erosion but also the effective slope exponent (DiBiase & Whipple, 2011; Lague, 2014). While the roles of both orographic precipitation and stochastic climate in stream power have each generated a lot of studies on their own, there has been less effort examining them together.

Integrating orographic effects with stochastic runoff into stream power models requires better constraints on how mean runoff and runoff variability are related (or unrelated) to each other via topography. Prior studies show that mean runoff and the shape of daily runoff distributions are correlated with each other in rainfall-dominated systems (Molnar et al., 2006; Rossi et al., 2016). Figure 1b illustrates this for the contiguous United States using streamflow data from select watersheds where the impact of human disturbance and management has been minimized (Figure 1a). To select watersheds to motivate and validate the global water model data that we use for most of this effort (described in greater detail later), we used the Geospatial Attributes of Gages for Evaluating Streamflow (GAGES-II) reference gauges and the Hydro-Climatic Data Network (HCDN-2009). HCDN-2009 is a subset of GAGES-II and thus includes a smaller number of sites. Details for the selection of the stations used for validation are described below along with how we derived the shape parameters of each distribution. However, note here that the higher shape parameters shown in Figure 1 indicate lower runoff variability. The empirical data were split into two broad relationships. The separation of the two trends appears to correspond to mean annual temperatures of around 0–10°C (Figure 1b), which we hypothesize is due to relatively small changes in the fraction of mean annual streamflow that is derived from snowmelt. While prior work has examined how orographic patterns in the spatial distribution of snow alter stream power predictions (Anders et al., 2008), we are not aware of any studies showing how snowmelt alters stochastic runoff and stream power predictions. As such, coupled models of climate and tectonics using stream power (e.g., Beaumont et al., 1992; Willett, 1999) may be missing important feedback between topographic relief and snowmelt as mountain ranges grow.

The lack of focus on integrating orographic precipitation and stochastic runoff into stream power models is likely due to data limitations and the dearth of simple hydrological relations that can be upscaled to landscape evolution timescales. Precipitation observations provide a starting point though simplifying water inputs into streamflow outputs is riddled with nonlinearities that can be hard to generalize. Rainfall runoff is nonlinear due to scaling properties within watersheds and dynamic nonlinearities in hillslope runoff generation (e.g., Sivapalan et al., 2002). Furthermore, the relative contribution of different runoff generation mechanisms (i.e., extreme precipitation, soil moisture excess, snowmelt) to flood frequency is only beginning to be characterized under modern climate conditions (e.g., Berghuijs et al., 2019), let alone for time-varying ones. Process-based hydrological models help unpack these nonlinearities for a given setting (Fatihi et al., 2016) but are typically applied at small spatial scales. Our approach is to use a global water model (Alcamo et al., 2003; Döll et al., 2003) to help constrain how topography, runoff generation, and streamflow statistics can be generalized for river incision modeling more broadly.

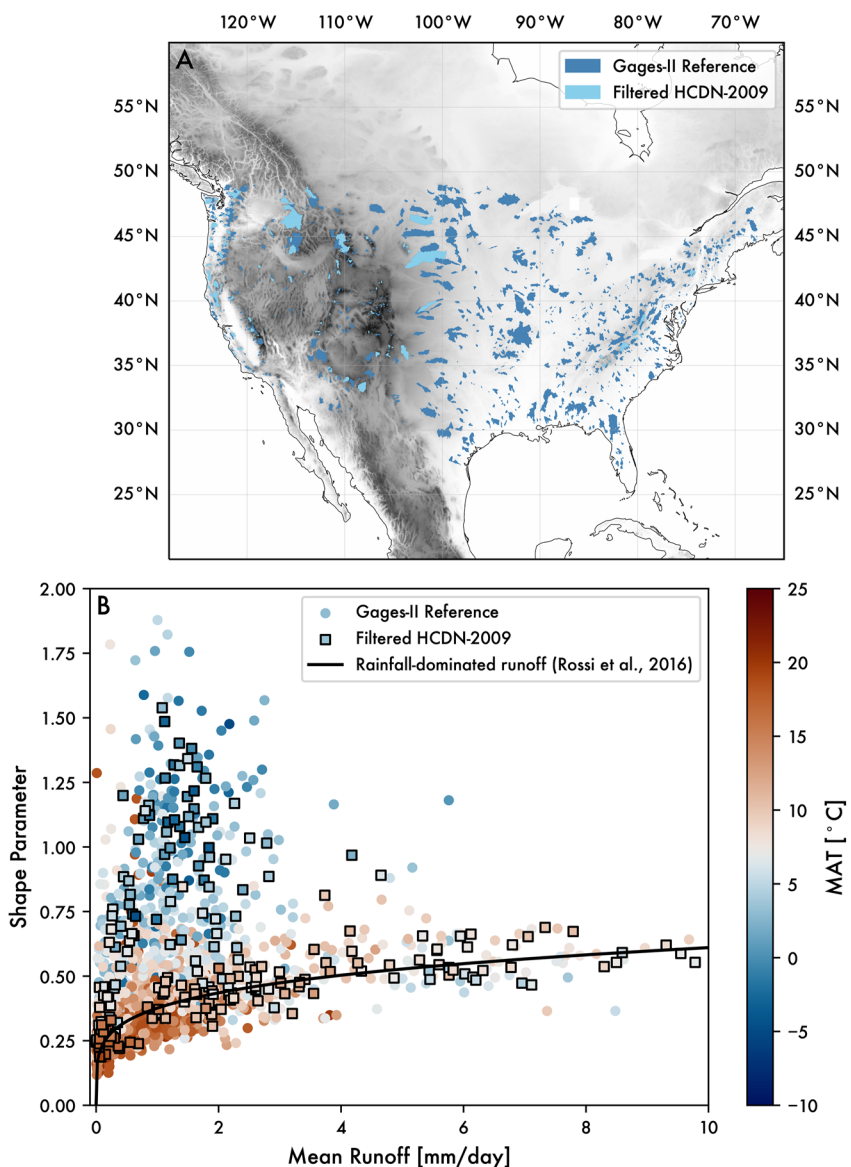


**Figure 1.** Observational stream gauge data used in this study includes (a) gauged sites in the contiguous United States that are minimally impacted by human management, which are then used to characterize (b) the relationship between mean runoff and the shape parameters describing daily runoff distributions for each stream gauge. In panel (a), a subset of the reference stations in the GAGES-II network were used for the water model validation presented below (i.e., filtered HCDN-2009). In panel (b), two broad trends between mean runoff and daily runoff variability organize around mean annual temperature, which prior authors have interpreted as reflecting the transition from snowmelt-dominated to rainfall-dominated systems (Rossi et al., 2016).

## 2. Background

### 2.1. Orographic Effects

Topography perturbs the equilibrium structure of the atmosphere by adding roughness, obstructing air masses, and serving as a heat source (Smith, 1979). The conventional treatment of orographic precipitation in landscape evolution studies (e.g., Beaumont et al., 1992; Willett, 1999) focuses on the thermodynamic implications of mountain topography on how precipitation is extracted from the atmosphere via forced ascent. The saturation vapor pressure of water in air is related to its temperature via the Clausius-Clapeyron equation (see review in Roe (2005)). As air masses move up and over mountain topography, precipitation on windward slopes increases as partially saturated air cools during ascent. A “rain shadow” subsequently develops when the relatively drier

air descends and warms on leeward slopes. This first-order description is well-rooted in atmospheric physics and observations (Barros & Lettenmaier, 1994). To extend these dynamics to air parcels flowing over more complex terrain, Smith and Barstad (2004) developed a linear model of orographic precipitation that accounts for atmospheric dynamics, upwind advection, and downslope evaporation. In this context, linearity does not refer to a single function describing rainfall but is instead a property of the system of differential equations used such that they are analytically tractable. Because settling velocities of snow are an order of magnitude lower than rain, this model can be used to examine how snow alters the spatial distribution of water inputs (Anders et al., 2008). However, one notable limitation to the linear model of orographic precipitation is that it does not account for the blocking of air by terrain, a nonlinear process that depends on the Brunt-Vaisala frequency describing the horizontal propagation of waves, horizontal windspeed, and orogen-scale relief (Barros & Lettenmaier, 1994; Galewsky, 2009; Jiang, 2003). Given that one of the key targets of landscape evolution models is to couple topography to climate through time, linear models of orographic precipitation are perhaps best suited to smaller mountain ranges.

Another approach toward characterizing orographic precipitation is to use climatological observations, especially since the advent of satellite-based remote sensing. For example, the Tropical Rainfall Measuring Mission (TRMM) was spaceborne for 17 years and provided new insights into complex spatial patterns in rainfall set up by high topography (e.g., Bookhagen & Burbank, 2006; Bookhagen & Strecker, 2008; Deal et al., 2017; Forte et al., 2016; Nesbitt & Anders, 2009). One of the key insights from these studies is the central importance of local relief in driving spatial patterns in rainfall. For example, in the Himalaya, TRMM rainfall revealed two narrow bands of rainfall that correspond to abrupt physiographic transitions into the Lesser Himalaya and into the Greater Himalaya, which had not been previously identified (Bookhagen & Burbank, 2006, 2010). As such, spatial patterns derived from TRMM rainfall are increasingly being used to inform interpretations of river channel profiles (Adams et al., 2020; Bookhagen & Strecker, 2011; Leonard et al., 2023), though these approaches typically assume mean rainfall is directly proportional mean runoff. While other remote sensing products like MODIS can also help constrain snow cover to construct a full water budget (Bookhagen & Burbank, 2010), such products tend to require temperature-index or process-based hydrological models to reliably estimate snowmelt contributions to streamflow (Walter et al., 2005).

Given the importance of snowmelt to streamflow in mid-latitude mountain ranges (Barnett et al., 2005; Barnhart et al., 2016), the difficulty of obtaining direct estimates of snowmelt leads to substantial uncertainty when using remotely sensed rainfall data as a proxy for runoff. Altering the phase of precipitation can cause up to 100% reductions in snowmelt contributions to streamflow in settings near the freezing temperature window (Adam et al., 2009). This has prompted some authors to suggest that climate change driven reductions in snowmelt fraction generally lead to lower streamflow as snowfall gives way to rain (Berghuijs et al., 2014). Such arguments rest on the premise that snowmelt runoff will lead to higher runoff ratios, all other things being equal, because solid water is stored in the snowpack and released more slowly than rainfall runoff. Better understanding of orographic effects on the snowmelt contribution to streamflow in mountain landscapes is sorely needed to improve stream power models of river incision.

## 2.2. Stochastic River Incision

Early efforts to integrate stochastic hydrology into stream power models of river incision (Snyder et al., 2003; Tucker, 2004; Tucker & Bras, 2000) were based on the pioneering work of Eagleson (1978). By simulating rainfall events as Poisson distributions of intensities, durations, and inter-storm periods, rainfall events were represented as rectangular pulses that can be converted to runoff and routed across the landscape in order to evaluate the impact erosion thresholds on landscape evolution. Complementary efforts by Lague et al. (2005) chose to simulate streamflow directly at the daily time step using the stochastic “precipiton” model. This model considers the time travel distribution of the quanta of precipitation that produces runoff and generates daily streamflow distributions that follow an inverse gamma distribution (Crave & Davy, 2001).

Despite the differences in the hydrologic assumptions made by these early modeling efforts, together they highlighted the need for adding stochastic events to stream power in order to interpret the long-term evolution of river profiles. Under this view, the steady state form of river profiles was no longer a simple function of mean climate, but instead reflected the complex interplay between the frequency of large flows and erosional thresholds set by coarse sediment (Shobe et al., 2016) and the detachment of bedrock (Whipple et al., 2000). While the overall

approach of these efforts was similar, the functional form of probability distributions of streamflow differed. The use of daily data, while insufficient for short-duration flash floods, balances important tradeoffs in characterizing magnitude-frequency relationships while also being tractable to simulate over landscape evolution timescales. Poisson rectangular pulses always generate light-tailed, exponential, daily runoff distributions, while the inverse gamma distribution is able to produce heavy-tailed distributions that do not have a finite variance, depending on the value of the shape parameter. There is still an open question as to how heavy-tailed streamflow distributions truly are (Malamud & Turcotte, 2006; Molnar et al., 2006), though the advantage of adopting these stochastic frameworks is that they are well-suited to simulating both frequent and infrequent flows and thus determining the geomorphically effective event (Huang & Niemann, 2006). Rossi et al. (2016) recently suggested that the stretched exponential, or Weibull, distribution provides a flexible probability distribution that spans light-tailed to apparently heavy-tailed distributions (Laherrère & Sornette, 1998), and thus is what we choose to fit observed and model runoff daily runoff data below.

Regardless of how stochastic processes are represented, these early efforts prompted a large number of studies to take a closer look at whether relationships between long-term erosion rates and river morphology can be better explained using stochastic-threshold models of river incision (Campforts et al., 2020; Desormeaux et al., 2022; DiBiase & Whipple, 2011; Forte et al., 2022; Scherler et al., 2017). While success is decidedly mixed, the general outcome of using stochastic-threshold models has been to provide an alternative interpretation to nonlinear relationships between river channel morphology and long-term erosion rates (Harel et al., 2016; Marder & Gallen, 2023). In these cases, nonlinear relationships between river morphology and long-term erosion rates arise because erosional thresholds are exceeded more frequently as erosion rate and relief increase. The climate driver on river profile evolution is not the annual precipitation itself but how the soil water balance (Deal et al., 2018) and the hydrologic structure of watersheds (Basso et al., 2023) mediate flood frequency. These concepts place the central focus on water storage-discharge relationships (Botter et al., 2009; Kirchner, 2009) to condition how rainfall events are converted to runoff ones. The same kind of framework can be used to account for seasonal snowmelt contributions to streamflow (Schaeefli et al., 2013).

### 3. Data Sets

Our overarching goal is to better parameterize 1D models of fluvial profile evolution that account for both stochastic events and orographic controls on runoff generation. Model development is the focus of our companion manuscript (Forte & Rossi, 2024a). The focus of this manuscript is on developing empirical relationships between topography and daily runoff statistics in mountain settings. Note that runoff and streamflow, that is, discharge, are not synonymous terms. For empirical data, streamflow data are typically what is measured and runoff is inferred by normalizing the data by drainage area. For water model data, runoffs are simulated directly. We primarily rely on three data sets: (a) a daily global water model derived from climate reanalysis data (WaterGAP3 data including daily runoff), (b) observational stream gauge data from the contiguous United States (HCDN-2009 daily streamflow), and (c) near global topographic data (SRTM-90 and derived HydroSHEDS v1 gridded elevation).

#### 3.1. Hydrology Data

Because streamflow data availability and quality are globally variable, we sought a single global runoff data set that could be used to interrogate modern relationships among topography, snowmelt, and runoff. We used the Water Global Assessment and Prognosis (WaterGAP3), the most recent version of a 20+ year old global water model (Alcamo et al., 2003; Döll et al., 2003). WaterGAP3 improves on prior versions by increasing the spatial resolution from the original  $0.5^{\circ}$ – $0.25^{\circ}$  pixel size (Eisner, 2015) and is one model included in the Earth2Observe Water Resource Reanalysis project (Schellekens et al., 2017). These model data have broad utility (e.g., Schmid et al., 2014), including for parameterization of stochastic-threshold incision models of river incision (Campforts et al., 2020). For this analysis, we downloaded the global, 20-year, daily time series from the Earth2Observe portal ([www.earth2observe.eu](http://www.earth2observe.eu); last accessed 8 April 2022) spanning from 1 January 1980 to 31 December 1999. Daily data represent the mean value of each variable for each day.

For each pixel and day, WaterGAP3 contains a large number of input and derived hydro-parameters, including precipitation, runoff, discharge, and evapotranspiration. We primarily focus on the derived runoff variables from WaterGAP3 but also briefly consider temperature and precipitation. Daily average surface temperature

is not distributed with WaterGAP3, so we rely on another reanalysis product of identical resolution from the Earth2Observe set, namely SURFEX-TRIP (Decharme et al., 2010, 2013). Surface temperature data are used to help interpret variations within the WaterGAP3 runoff data. Runoff data are subdivided into three components in WaterGAP3: surface runoff ( $R_s$ ), subsurface runoff ( $R_{sb}$ ), and snowmelt ( $R_{sm}$ ), where total daily runoff ( $R_t$ ) is the sum of the three. In the original WaterGAP3 data set, all of these components of runoff are denoted by the variable “ $Q$ .” We do not use this notation here given the common association of  $Q$  with discharge [ $L^3/t$ ] as opposed to runoff [ $L/t$ ]. For each pixel across the time-series, we calculated mean daily runoff ( $\bar{R}_t$ ), mean daily precipitation ( $\bar{P}$ ), means of each of the three runoff components ( $\bar{R}_s$ ,  $\bar{R}_{sb}$ ,  $\bar{R}_{sm}$ ), and Weibull shape ( $c$ ) and scale ( $R_0$ ) parameters of the daily total runoff distributions (see Section 4.1 for details). Given our interest in probing the importance of snowmelt, we also calculated the fraction of runoff contributed by snowmelt (SF), where:

$$SF = \frac{\bar{R}_{sm}}{\bar{R}_t} \quad (1)$$

Similarly, we calculate baseflow fraction of runoff (BF), where:

$$BF = \frac{\bar{R}_{sb}}{\bar{R}_t} \quad (2)$$

that we use to exclude watersheds with a substantial groundwater component from its daily fluxes.

To validate model runoff data, we used observational streamflow data from the Hydro-Climatic Data Network—2009 (HCDN-2009) (Lins, 2012). These 743 stream gauges were identified by the USGS to be high quality, long, continuous records for watersheds with minimal impact by humans (e.g., due to landcover change, dams, and diversions). We downloaded streamflow data from the National Water Information System server for the dates between 1 January 1980 and 31 December 1999, to compare directly with the WaterGAP3 data. During the processing of individual HCDN-2009 time series data, any day that included provisional data or data where there was an extra qualifier on the quality (e.g., “ICE”) was removed and treated as NaN data. We characterize the completeness of the time series by dividing the number of days with reliable data by the total number of days. Because HCDN-2009 stream gauges are a subset of the reference stations in the Gages for Evaluating Streamflow version II (GAGES-II) network, we were able to use watershed boundaries provided by Falcone (2011) to calculate watershed-averaged properties and normalize streamflow by drainage area. This latter calculation was used as an estimate for daily runoff. Processing and validation of the WaterGAP3 runoff model against HCDN-2009 observations is described in Section 4.2.

### 3.2. Topography Data

Because we are focused on how hydroclimatic parameters vary with topography in mountain settings, it is necessary to pair the WaterGAP3 data with a global topographic data set. We largely used the HydroSheds v1, 15-arcsecond, digital elevation model (DEM) that is derived from SRTM elevation data (Lehner et al., 2008). We also used the higher resolution SRTM-90 data (Farr et al., 2007) for watershed delineation when validating WaterGAP3 against HCDN-2009 data. The HydroSheds v1 topographic data are used for two purposes: (a) to screen for portions of the global surface where orographic feedbacks with climate are relevant, and (b) to develop empirical relationships between topography and runoff statistics. With respect to data screening, we only used WaterGAP3 data where the mean elevations are greater than 250 m above sea level and where local reliefs are greater than 500 m. To calculate local relief at a fixed scale, we first reprojected the global geographic DEM into an equal area cylindrical projection and then calculated local relief within a 2.5 km radius circular moving window. This is a scale that prior studies have shown to linearly correlate with river channel steepness (e.g., DiBiase et al., 2010), and thus we expect it to be well suited to developing empirical relationships between river morphology and local relief. After the relief calculation, we projected the data back into the original WGS 84 geographic coordinate system to facilitate calculation and comparisons with the rest of the data sets that were also in geographic coordinate systems. The initial screening of the WaterGAP3 data using local relief is then further filtered to exclude pixels where baseflow (Equation 2) exceeds 0.25, with an eye toward minimizing the confounding factor of large groundwater contributions. To develop relationships between topography and runoff statistics, we record minimum, mean, and maximum elevations within a WaterGAP3 pixel and the mean local

relief within a WaterGAP3 pixel as calculated from the enclosed 60 HydroShed pixels (i.e., there are 60 HydroShed pixels within each WaterGAP3 pixel).

## 4. Data Analysis

To develop empirical relationships between topography and runoff statistics from WaterGAP3, it was first important to figure out at which scale such relationships might emerge. To this end, we conduct both a global analysis and a set of regional ones that broadly correspond to the mountain range scale. These empirical relationships serve as the basis for the model development and analysis we conduct in Part 2 (Forte & Rossi, 2024a). There are four main steps to the data analysis: (a) Characterization of statistical parameters for daily runoff; (b) Validation of WaterGAP3 model derived parameters with HCDN-2009 stream gage observations; (c) Global assessment of topographic controls on runoff, runoff variability, and snowmelt fraction; and (d) Development of regionally-based relationships between topographic metrics and runoff statistics.

### 4.1. Daily Distributions

A number of probability distributions have been considered for the problem of bedrock river incision, including exponential (Snyder et al., 2003; Tucker, 2004), power law (Molnar et al., 2006), inverse gamma (Campforts et al., 2020; DiBiase & Whipple, 2011; Lague et al., 2005; Scherler et al., 2017) and Weibull (Forte et al., 2022; Rossi et al., 2016) distributions. We follow Rossi et al. (2016) and use a two-parameter Weibull distribution to fit the right tail of the daily runoff distribution above a threshold value. Choosing thresholds to fit empirical distributions is a notoriously vexing challenge (e.g., Dupuis, 1998) and makes it more challenging to implement in numerical models (see Forte & Rossi, 2024a), though it enables better fidelity to the observed right tail. For this analysis, the threshold is treated as a third parameter that is held constant across sites to enable comparison of fit parameters. Above the threshold, distributions are described by a shape parameter ( $c_x$ ) that describes daily variability and a scale ( $x_0$ ) parameter related to the mean of the distribution, where:

$$\text{pdf}(x; x_0, c_x) = \frac{c_x}{x_0} \left( \frac{x}{x_0} \right)^{c_x - 1} \exp^{-1}(x/x_0)^{c_x} \quad (3)$$

Because we are only fitting the right tail of the distribution, the parametric mean and the empirical mean need not match. The mismatch between the two is a measure of how well tail fitting is able to represent the full distribution. We use the fit parameters to characterize both daily precipitation ( $p_0, c_p$ ) and daily runoff ( $r_0, c_r$ ). Interpretations of fit parameters primarily focus on the shape parameter because it describes the right tail of daily values, which we colloquially refer to as the variability. Larger values of  $c_x$  indicate lower variability (i.e., smaller relative differences between daily runoff values), where  $c_x = 1$  is equivalent to the exponential distribution. The need for three parameters and the inability to analytically integrate the product of this distribution with stream power is not ideal, posing important challenges to numerical simulations of bedrock rivers (Forte & Rossi, 2024a).

To estimate shape parameters, we follow Wilson and Toumi (2005) and perform a linear fit on the natural log linearized right tail of the exceedance frequency distribution above a threshold. On the transformed data, the shape parameter,  $c_x$ , is the slope of the regression, and the scale parameter,  $x_0$ , is  $\exp(-\text{intercept}/\text{slope})$  of the regression. Because parametric fits are sensitive to threshold choice, distribution parameters were calculated using two thresholds for the daily runoff data: the upper 5% and upper 1% of daily values. These thresholds reflect a compromise between fitting the majority of flows while also honoring the right tail, the latter of which dictates the nonlinear relationship between channel steepness and long-term erosion rates. Figures and discussion are based on the 1% threshold for both runoff and precipitation distributions. This corresponds to the event magnitude that happens 3–4 times per year. While threshold choice did alter the best-fit values for  $c_r$ , suggesting that a simple Weibull distribution is not able to fully characterize all cases, this variation in  $c_r$  did not substantially alter the relative spatial patterns in the shape of the right tail. Runoff parameters were calculated on both the daily streamflow data (HCDN-2009) and the daily total runoff data from WaterGAP3. Pixel-based values in WaterGAP3 are not directly comparable to the watershed-averaged ones in HCDN-2009. In the following section, we address this challenge in the context of validating water model runoff data against observations.

#### 4.2. Runoff Parameter Validation

Prior validation of WaterGAP3 data suggests that model data robustly reproduce mean river discharge from gauging stations (Beck et al., 2017; Eisner, 2015; Schmied et al., 2014, 2020). None of these prior assessments considered how well daily runoff variability is represented. Given the importance of daily runoff variability to bedrock river incision modeling, it is thus important to assess the extent to which shape parameters calculated from WaterGAP3 are consistent with those observed at stream gauges. For the sake of comparison, we first screened the HCDN-2009 network using the same topographic criteria used to screen WaterGAP3. Namely, we excluded watersheds where catchment relief (i.e., maximum minus minimum elevation within the catchment) is less than 500 m and where mean elevation is less than 250 m. Of the retained sites, we also imposed the additional criterion that HCDN-2009 daily runoff records are >95% complete within the WaterGAP3 time period (1 January 1980–31 December 1999). We also removed data that occur on leap days because these days are not calculated in the WaterGAP3 time series.

Once candidate HCDN-2009 stations were identified for validation, we needed to process the WaterGAP3 data to enable fair comparison. The first approach uses the mean runoff and runoff variability parameters calculated for each pixel in WaterGAP3. By oversampling these raster data sets of stochastic parameters to 1.5 s per pixel, HCDN-2009 watershed boundaries were used to calculate spatially averaged values of runoff parameters. While this treatment may be valid for small HCDN-2009 watersheds of similar scale to the WaterGAP3 pixels, this calculation may be problematic for larger watersheds where runoff should be routed downstream. As such, the second approach uses watershed boundaries to clip and route the WaterGAP3 data for each day within the 20-year time series. The mean runoff and shape parameter of the routed data are then calculated for the daily routed data at the river outlet. For this computationally intensive approach, we used TopoToolbox (Schwanghart & Scherler, 2014) to: (a) acquire SRTM-90 DEMs for each watershed via the OpenTopography API, (b) project each DEM to the Universal Transverse Mercator projection, (c) clip each day of the WaterGAP3 data to the watershed boundary and resample to the resolution of the DEM, (d) route discharge through the basin to build a time series of daily runoff at the outlet of each watershed, and (e) calculate mean runoff and shape parameters for the outlet time series.

#### 4.3. Global Analysis

After understanding the strengths and limitations of WaterGAP3, these model data were used to identify the strongest predictors of mean runoff and daily runoff variability globally. The global analysis used two complementary approaches: (a) Develop relationships between mean runoff and variability (e.g., Molnar et al., 2006; Rossi et al., 2016) in a way that can account for the potential influence of snowmelt, and (b) Use unsupervised machine learning to probe the WaterGAP3 data and help identify strong predictors of mean runoff, snowmelt, and runoff variability.

For the first approach, we used the snowmelt fraction (Equation 1) to partition the filtered WaterGAP3 data (see Section 3.1) into bins. Within each bin, we fit both a linear and a power law function relating mean runoff and the shape parameters of each pixel within that bin. This approach was motivated by empirical (Rossi et al., 2016) and ecohydrological modeling (Deal et al., 2018) studies that show how climatically driven gradients in daily runoff variability differ between rainfall-runoff and snowmelt-runoff regimes. For example, Rossi et al. (2016) showed that watersheds with lower snowmelt contributions were better described by a power law relationship between mean runoff and its associated Weibull shape parameter. In contrast, regions with higher snowmelt contributions showed a more linear relationship between these parameters. To compare the fits of both functions, we consider both the RMSE and the reduced chi-square statistic under the view that minimization of RMSE and/or reducing the chi-square statistic closer to one should indicate the “better” fit to the data.

In the second approach, we consider a larger suite of hydroclimatological, topographic, and geographic variables. Random forest regression (RFR) was used to assess the relative importance of potential predictor variables with respect to a given “target” variable (Grömping, 2009). Target variables are hydroclimatic ones chosen based on their potential relevance to the relationship between mean runoff and runoff variability (i.e., mean temperature, mean precipitation, mean runoff, daily runoff variability, and snowmelt fraction). The list of predictor variables is broader and varied according to each target. Predictor variables included topographic (mean elevation, maximum elevation, mean local relief), geographic (latitude), and hydroclimatic (mean temperature, mean precipitation,

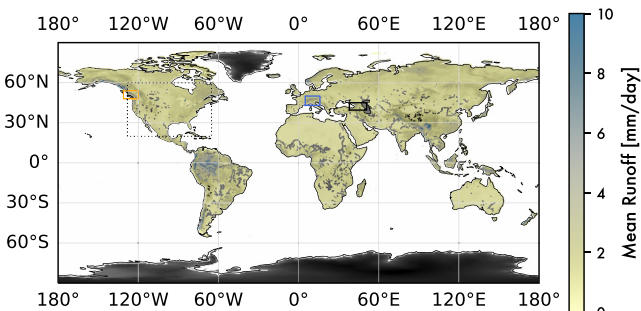


**Figure 2.** Global mean runoff from the WaterGAP3 water model (1980–1999). The dotted black box corresponds to the area shown in Figure 1a and bounds the geographic extent of the validation data used. The three smaller colored boxes show the geographic extent of the three mid-latitude regional case studies introduced in Section 4.4.

were difficult to isolate at this largest spatial scale. While the global analysis reinforced the notion that the snowmelt fraction mediates the relationship between mean runoff and daily runoff variability, scatter in these relationships clearly reflect the geographic diversity of montane hydrology. Furthermore, the lack of unambiguous topographic predictors that could be used to build rules for co-evolving stochastic parameters with the growth of mountain ranges limits the utility of the results from the global analysis to the application of 1D bedrock river incision modeling (Forte & Rossi, 2024a). As such, we identified relationships between topography and stochastic runoff specific to individual mountain ranges, where differences in regional climate and geography can be partially accounted for. To begin this regional analysis, we started at first at the global scale and used a  $2^{\circ}$  rectangular moving window to calculate the Spearman's rank correlation coefficient between candidate topographic variables and hydroclimatological variables. The topographic variables considered were the same as in the global analysis (mean elevation, maximum elevation, and mean local relief). The hydroclimatological variables we focused on were mean runoff and snowmelt fraction, the latter of which can be linked to daily runoff variability using relationships from the global analysis. We opt to focus on snowmelt fraction instead of daily runoff variability directly because one of the hypotheses we are trying to test in the 1D river incision modeling (Forte & Rossi, 2024a) is how and whether snowmelt dynamics alter interpretations of stream power based analyses of river profiles. The results of the rank correlation analysis were used as the basis of selecting three regions where well-defined relationships can be developed between topography and hydroclimate. Specifically, these regional cases focus on the mid-latitude mountains of British Columbia, the European Alps, and the Greater Caucasus (Figure 2), where snowmelt contributes a sizable fraction of daily streamflow.

## 5. Results

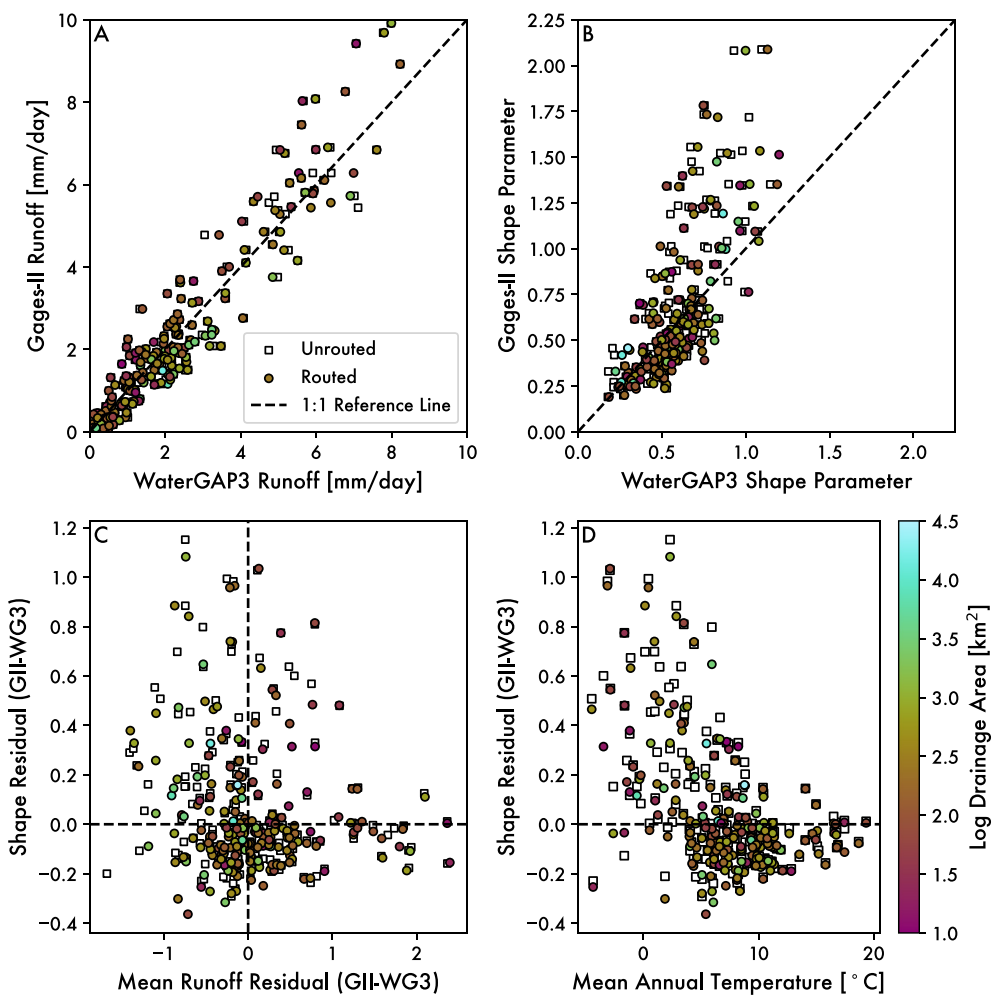
### 5.1. Validation of WaterGAP3

Figure 3 summarizes the results from our validation of WaterGAP3 model data against historical observations from select HCDN-2009 stream gages. The mean values for both data sets plot around the 1:1 line without obvious bias (Figure 3a), lending support to prior assessments (e.g., Beck et al., 2017; Eisner, 2015; Schmied et al., 2014, 2020). However, scatter around this relationship shows that a >25% mismatch in mean values is not unusual. In general, simple spatial averaging (closed symbols) performs almost as well as the computationally intensive routed approach (open symbols), though routing matters for individual cases. From this, we conclude that the HCDN-2009 watersheds are at the appropriate scale for WaterGAP3 validation and that downstream scaling of streamflow statistics is not strongly influencing our parameter estimates. This is perhaps not surprising given that the filtered set of HCDN-2009 watersheds used are relatively small (interquartile range of 105–542 km<sup>2</sup>), well within the average pixel size of the WaterGAP3 data and typically smaller than the mountain range scale. For lower values of the shape parameter (i.e., higher runoff variability), the correspondence between the observations and the water model is acceptable (Figure 3b). However, for most watersheds, the shape parameters from WaterGAP3 are less than their empirical counterparts (Figures 3b and 3d) except at higher shape parameters (i.e., lower daily runoff variability). In these cases, WaterGAP3 values are systematically lower than the HCDN-2009

daily precipitation variability, mean runoff, daily runoff variability, and snowmelt fraction) variables. We also attempted to thin predictor variables and remove what amounts to duplicates, for example, as described in the results, latitude is the primary predictor of mean annual temperature and thus for other RFRs, we only include MAT as opposed to both MAT and latitude. Ultimately, we are not interested in the prediction *per se* but to use the RFR to help identify which variables emerge as the most viable candidates linking mean runoff, snowmelt fraction, and daily runoff variability. In particular, we sought to discover which and whether any of the topographic metrics can be used to generalize hydroclimatic relationships that may co-evolve with growing topography. To perform the RFR, we used the *RandomForestRegressor* within *SciKit-Learn*, using the default values and a seed for the random state of 0.

### 4.4. Regional Cases

As we discuss in the context of our findings below, the global analysis revealed that generalizable relationships between topography and hydroclimatology



**Figure 3.** Comparison of WaterGAP3 runoff parameters against selected HCDN-2009 stream gage data, colored by the log of the drainage area of individual gaged basins: (a) Mean runoff values, (b) Shape parameters of daily distributions, (c) Mean and shape residuals with respect to 1:1 line, and (d) Shape residuals against mean annual temperatures for each watershed. Open squares represent arithmetic means of WaterGAP3 values within watershed boundaries. Closed and colored circles route daily WaterGAP3 data to generate a time series that is then used to calculate fit parameters. Dashed lines in the upper panels indicate a 1:1 relationship between the water model and gaged data, whereas dashed lines in the lower panels reflect a 0 residual value.

gage data. This implies that WaterGAP3 tends to *overestimate* variability for these watersheds. For the lower variability watersheds, the routed version of WaterGAP3 slightly improves water model performance (Figure 3b) but does not remove the systematic bias. The residuals of the mismatch between the HCDN-2009 and WaterGAP3 values do not reveal a relationship between the mean and variability (Figure 3c), which might occur if the WaterGAP3 model was systematically altering storage-release relationships in hydrographs (e.g., due to limitations in how hydrologic processes are represented in the model). However, comparison of the residuals of the shape parameter to the mean annual temperature the watershed (Figure 3d) indicates one possible interpretation for why variability in lower variability watersheds is overestimated in the WaterGAP3 data. The majority of lower variability basins tend to occur in colder settings, suggesting the possibility that snowmelt processes are not being adequately represented in the WaterGAP3 data. This result supports the argument that WaterGAP3 could benefit from improving the partitioning of runoff into fast and slow components (Eisner, 2015). The direction of the mismatch is consistent with the notion that snow storage and release may not be fully resolved in WaterGAP3 data even though mean runoff is well represented in the water model.

While systematic differences between model and empirical estimates of daily runoff variability is an important limitation to consider, we continue to use WaterGAP3 as our base data set for a few reasons: (a) It is globally

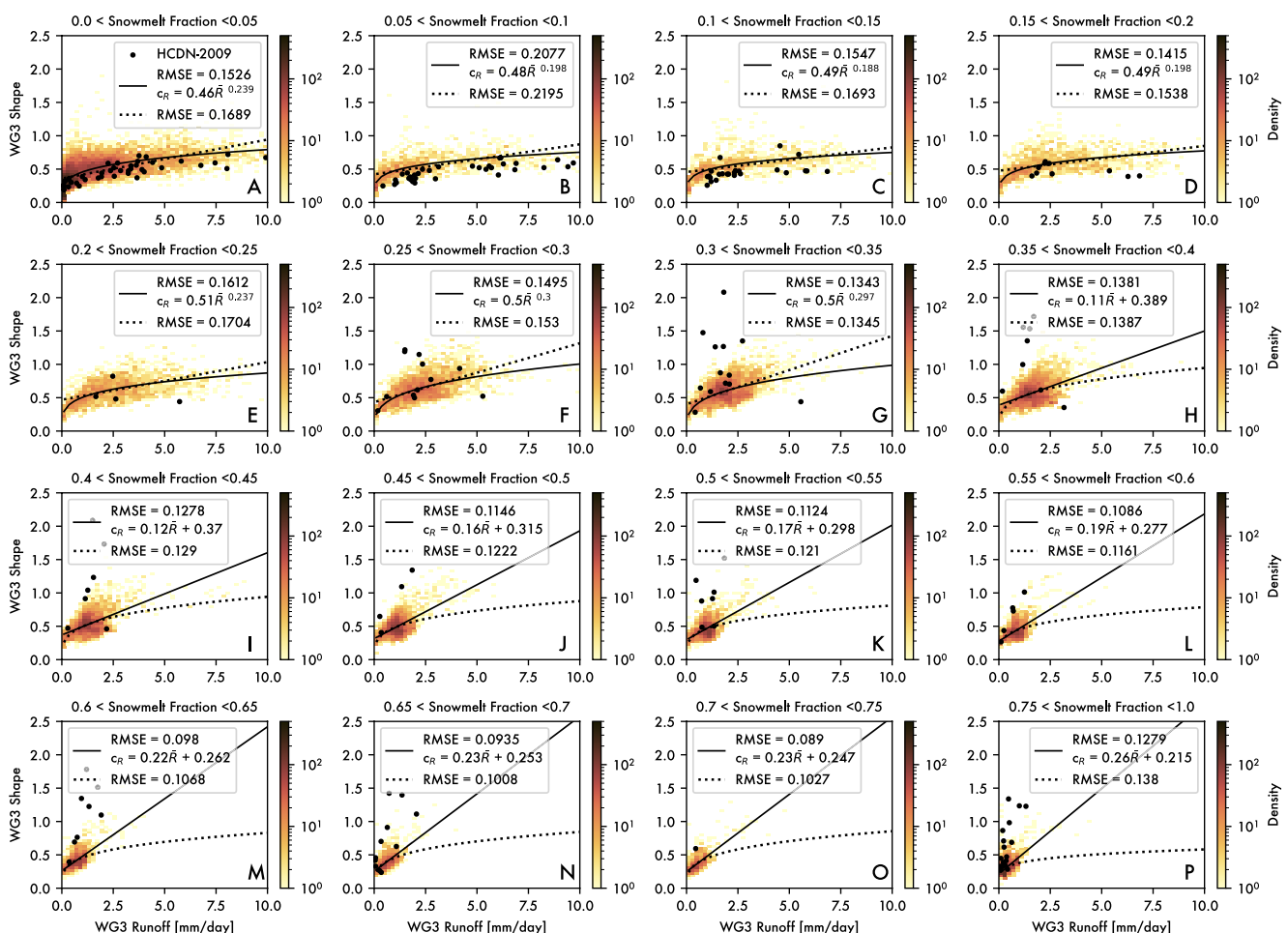


**Figure 4.** Density plots show the relationship between the shape parameter and mean runoff for the filtered WaterGAP3 data: (a–o) Plots binned by snowmelt fraction in increments of 0.05 up to 0.75 snowmelt. (p) The last panel is for the remaining data that have >0.75 snowmelt. In all panels, both a power law and linear fit are shown. The better fit is shown using a solid line and is based on having a lower RMSE. Results are the same if using the reduced chi-square statistic. Black dots are HCDN-2009 watersheds filtered in the same way. For HCDN-2009 data, the snowmelt fraction was taken from WaterGAP3 data.

uniform, allowing for the comparison of stochastic runoff in diverse settings, and (b) The systematic bias in variability has been quantified so that its effects can be considered. Importantly, the bias in WaterGAP3 estimates of daily runoff variability leads to a *conservative* estimate of the dynamics we are examining in our 1D modeling of bedrock river incision (Forte & Rossi, 2024a). Because hypothesized orographic feedback induce lower runoff variability as a mountain range grows, thereby increasing the degree of nonlinearity between channel steepness and erosion rate, it is preferable for the underlying rules setting these feedback to overestimate variability than the alternative.

## 5.2. Global Relationships (Relating Mean and Variability)

Figures 4 and 5 summarize the results for how the parametric fit parameters relate to mean runoff after binning the data by snowmelt fraction. Across all bins, WaterGAP3 data show that mean runoffs are inversely related to daily runoff variability, consistent with prior studies (e.g., Molnar et al., 2006; Rossi et al., 2016). The large gridded WaterGAP3 data set allowed us to more systematically explore these relationships at relatively fine (5%) intervals of snowmelt fraction (Figure 4). Each subplot in Figure 4 is a heatmap showing the density of WaterGAP3 observations of how the best-fit shape parameters relate to the empirical mean. Regressions on the pixel-level data are shown (solid lines show the better fit between linear and power law regressions). HCDN-2009 observational data are also shown as points for reference. Figure 4 demonstrates that it would be difficult to constrain these relationships using observational data alone because the representation of different snowmelt

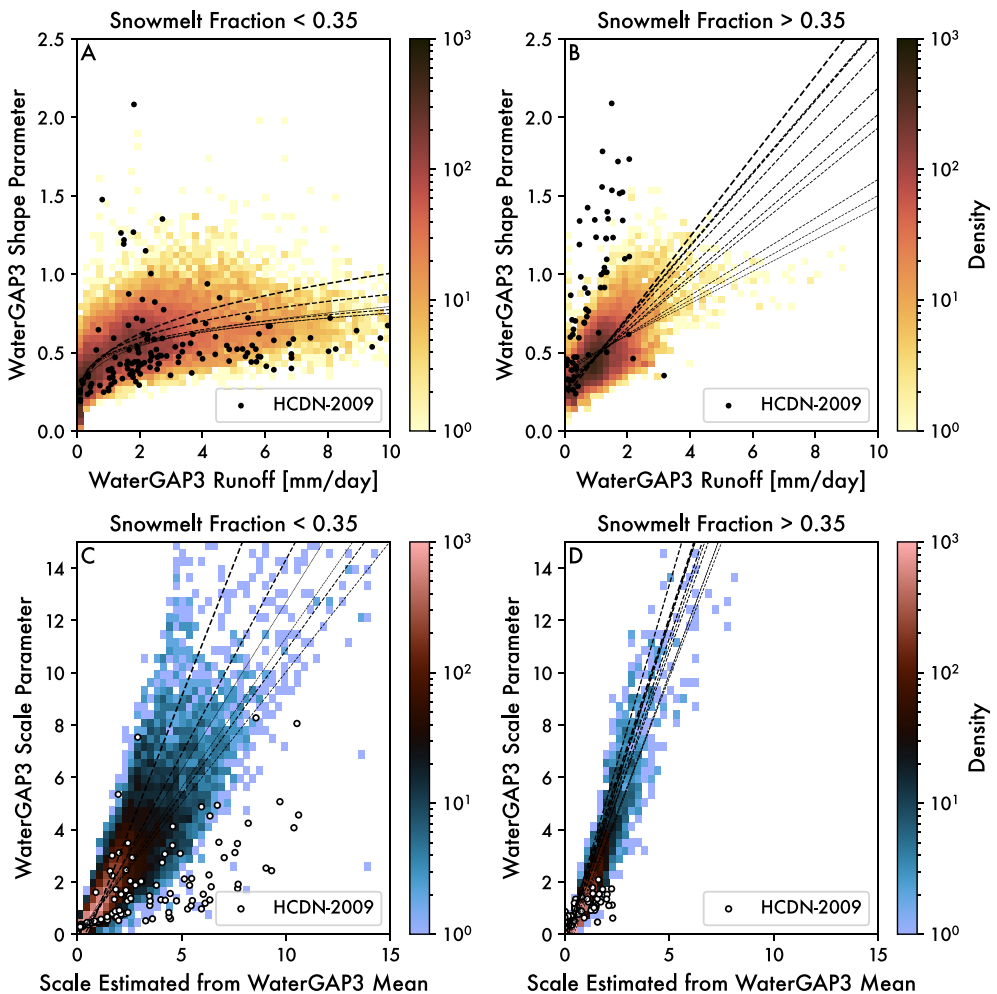


**Figure 5.** Density plots showing relationships among the scale and shape parameters of parametric fits with the mean runoff observed for the filtered WaterGAP3 data. (a) Relationship between mean runoff and shape of the right tail for pixels where the snowmelt fraction is  $< 0.35$ . (b) Relationship between mean runoff and shape of the right tail for pixels where the snowmelt fraction is  $> 0.35$ . Because parametric fits include a threshold, the mean of the distribution cannot be directly inferred from scale parameters. (c) Relationship between the scale parameters fit to the data versus those implied from the empirical mean for pixels where the snowmelt fraction is  $< 0.35$ . (d) Relationship between the scale parameters fit to the data versus those implied from the empirical mean for pixels where the snowmelt fraction is  $> 0.35$ . Black dots are HCDN-2009 watersheds filtered in the same way. The strongest regressions from Figure 4 (a and b) and Figure S1 in Supporting Information S1 (c and d) subpanels are shown for reference.

fractions can be sparse, especially at higher snowmelt fractions. More importantly, it shows that the functional form of the relationship between the mean and variability changes from sublinear to linear with increasing snowmelt fraction. Using Figure 4 as our guide, we identified a snowmelt fraction of 0.35 as the transition where sublinear relationships give way to linear relationships. Note that this transition is higher than the 10% snowmelt threshold used to delineate snowmelt from rainfall-runoff dominated watersheds in Rossi et al. (2016). This disparity likely arises from two factors. First, that prior analysis focused on the snow fraction of precipitation and not the snowmelt fraction of runoff. Second, the sparsity of observations at higher snowmelt fractions in the HCDN-2009 data is not sufficient to define such a threshold.

To more succinctly summarize these findings, Figures 5a and 5b show the same plots by binning the data above and below a threshold snowmelt fraction of 0.35. The best of the regression lines from Figure 4 are also plotted for reference. Figures 5a and 5b highlight that individual regressions largely cluster around each other, especially in the domain where they are well constrained by data. It also shows that the relative spread of parameter values is smaller when there is a high fraction of snowmelt. The linear relationships shown at higher snowmelt fractions

(Figure 5b) strongly underestimate the value of the shape parameter as estimated from gaged basins, consistent with validation results (Figure 3b). However, empirical observations still suggest a linear relationship between the empirical mean runoff and the shape of the daily runoff distribution at higher snowmelt fractions.

Because empirical means are not equivalent to the mean value implied by parametric fits, Figure S1 in Supporting Information S1 reports the mismatch between the scale parameter fit to the data (i.e., above the 1% threshold or ~4 largest floods per year) and the scale parameter implied by the empirical mean. These results are summarized in Figures 5c and 5d. In general, the parametric fits produce scale parameters that are on par with the empirical means only at low snowmelt fractions. At higher snowmelt fractions, the parametric fits have much higher scale parameters than the empirical mean would imply, thereby suggesting that the Weibull distribution is not doing a good job of describing the full distribution of events. Finding a single distribution to describe empirical data is a well-known problem and poses unique challenges to simulating runoff distributions over landscape evolution timescales, a challenge we tackle in Part 2 of this analysis (Forte & Rossi, 2024a). Nevertheless, by treating all the data in the same way, we show that the functional relationship between daily runoff variability and mean runoff is highly sublinear at low snowmelt fractions, much like what was shown in previous studies (Molnar et al., 2006; Rossi et al., 2016). At high snowmelt fraction, the relationship becomes more linear, albeit with the caveat that the form of the distribution may also be changing. Our estimates of this transition using WaterGAP3 data provide conservative estimates of orographic feedback on runoff variability where both the mean and snowmelt fraction are expected to increase as mountain topography grows. It is conservative because biases in the water model data tend to dampen contrasts between rainfall and snowmelt dominated hydrology, and thus our 1D bedrock river incision modeling uses rulesets with weaker feedback than might be expected in reality (Forte & Rossi, 2024a).

While analyzing the global water model data was motivated by prior studies that identified an inverse relationship between mean runoff and daily runoff variability in the contiguous U.S. (Molnar et al., 2006; Rossi et al., 2016), we felt it also important analyze the global data more generically and explore whether hydroclimatic parameters can be linked to topography itself. This latter objective is essential to building rules that relate stochastic runoff parameters to mountain range growth and decay. To this end, we opted to use RFR to partition the relative influence of topographic, geographic, and hydroclimatic predictors on a small subset of target variables.

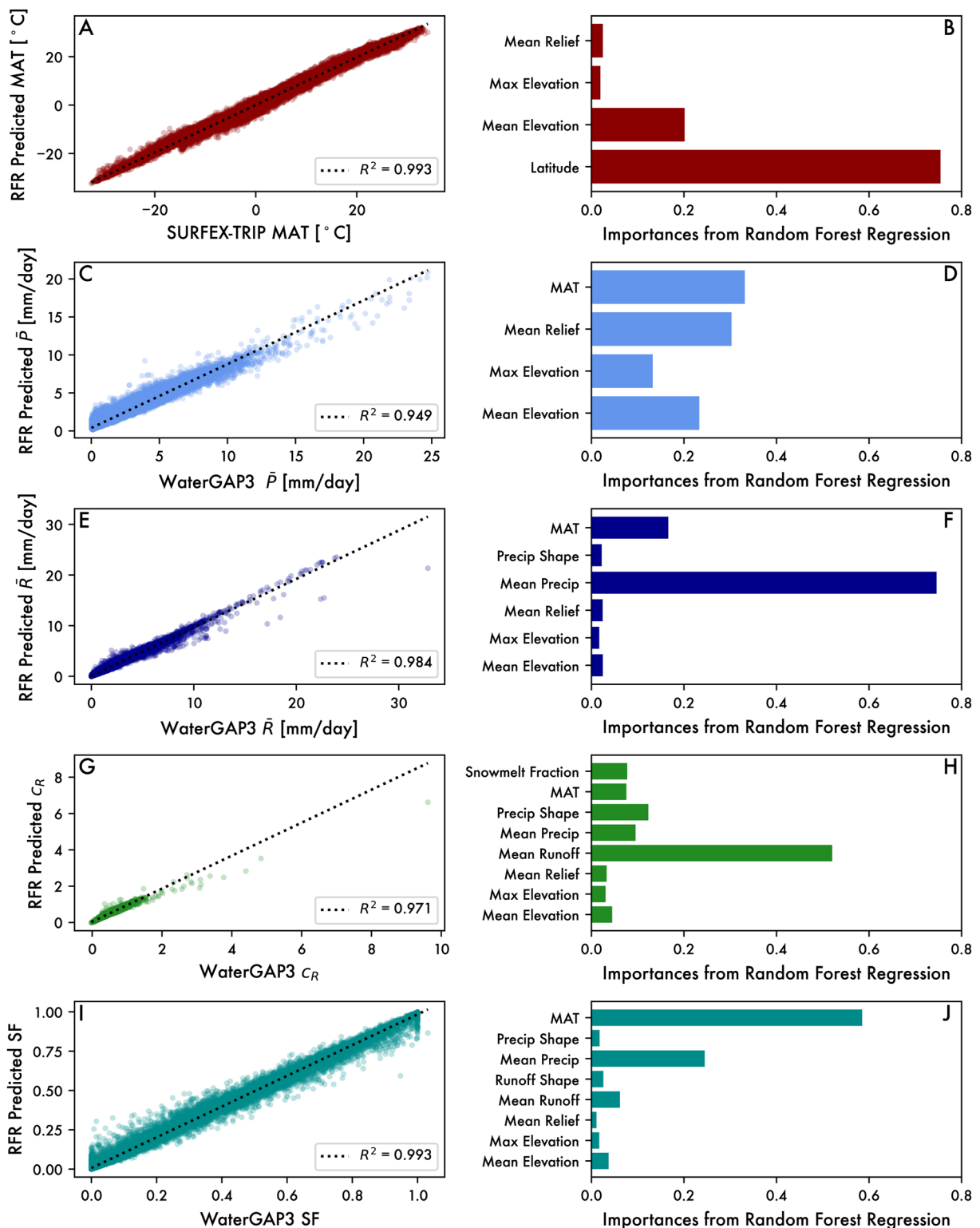
### 5.3. Global Relationships (Random Forest Regression)

Figure 6 summarizes the results of the RFR analysis performed on global filtered WaterGAP3 data. While principally interested in understanding the controls on mean runoff (Figures 6e and 6f), daily runoff variability (Figures 6g and 6h), and snowmelt fraction (Figures 6i and 6j), we also consider influences on other hydroclimatological variables that emerged as important determinants of these target variables, specifically mean annual temperature (Figures 6a and 6b) and mean precipitation (Figures 6c and 6d). The results of the RFR are not particularly surprising but do shed some light on potential causal chains that link mean runoff, snowmelt fraction, and daily runoff variability as a mountain range grows.

Mean annual temperature and mean precipitation are the two strongest predictors of both mean runoff and snowmelt fraction, with temperature exerting a stronger influence on snowmelt fraction and precipitation exerting a stronger influence on runoff. Mean runoff is the strongest predictor of the shape of the daily runoff distribution, perhaps explaining why prior efforts have focused on this relationship (e.g., Molnar et al., 2006; Rossi et al., 2016).

Importantly, topographic metrics were weak predictors of all three principal targets (mean runoff, snowmelt fraction, and daily runoff variability). This may be due to the fact that topography is expected to exert its influence via precipitation and temperature. To assess this, we also set mean precipitation and temperature as target variables in the RFR. The relative predictive power of the three topographic metrics and mean temperature on mean precipitation is relatively uniform. In contrast, latitude is the strongest predictor of mean temperature, with mean elevation providing modest predictive power. At this scale of analysis, topography does not appear to emerge as a strong predictor in the RFR modeling.

To further probe how topographic relationships might be obscured in this global analysis, we binned the pixel-level data by its mean temperature and precipitation, which emerged above as first-order controls on snowmelt fraction and mean runoff. We first removed outlier values using the method described by Doane (1976), where bin boundaries are defined after clipping variables to values below the 99.9th percentile. Membership in a given bin was determined by the mean temperature and precipitation of the pixel in question. Within each temperature-precipitation



**Figure 6.** Results from the random forest regression for predicting (a and b) Mean Temperature, (c and d) Mean Precipitation, (e and f) Mean Runoff, (g and h) Runoff Variability, and (i and j) Snowmelt Fraction. For each target variable, the left plot compares observed versus predicted data (linear fit with  $R^2$  shown for reference), and the right plot shows the relative importance of predictors.

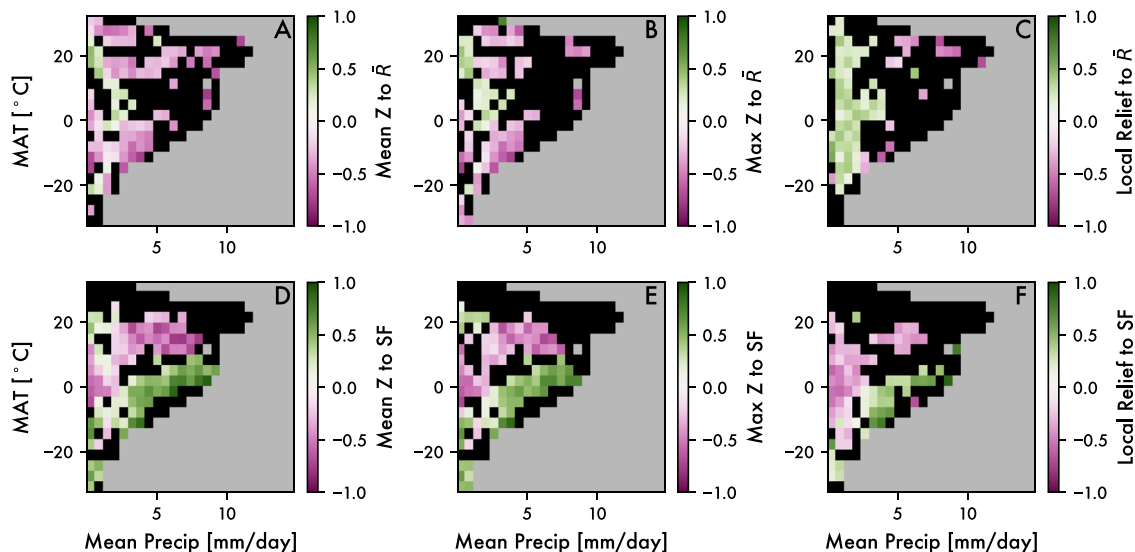


**Figure 7.** Spearman's rank correlation coefficients within temperature–precipitation bins. (a–c) Coefficients relating topography and mean runoff. (d–f) Coefficients relating topography to snowmelt fraction. The topographic variables considered were (a and d) mean elevation, (b and e) maximum elevation, and (c and f) local relief. For all plots, the gray area indicates regions of parameter space with less than 10 observations. Black regions indicate that there were more than 10 observations, but that the correlation did not exceed the 95% confidence interval. Note that these plots obscure the number of observations in each precipitation–temperature bin. As such, see Figure 8 to assess the distribution of correlation coefficients within their spatial context.

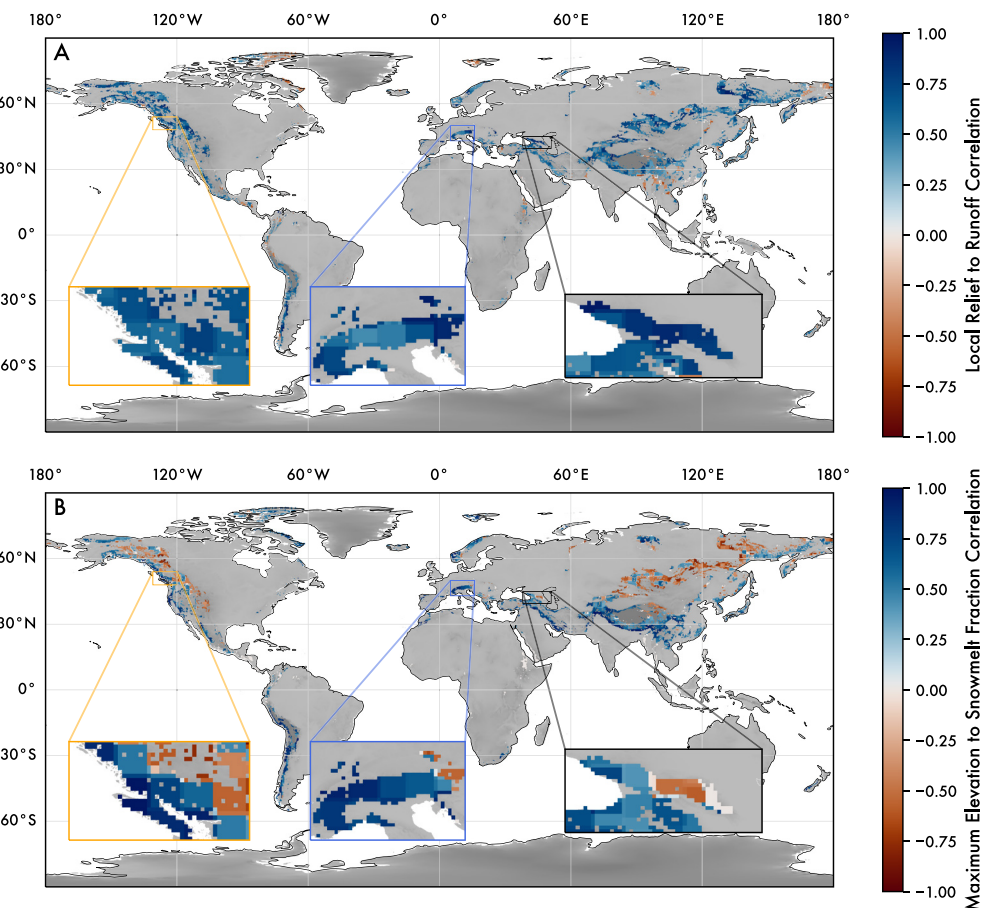
bin, we calculated Spearman's rank correlation coefficient between one of three topographic metrics (mean elevation, maximum elevation, and mean local relief) and either the mean runoff or snowmelt fraction. A correlation coefficient is calculated only if there are at least 10 pixels within a given temperature–precipitation bin and if the significance of the correlation coefficient exceeds the 95% confidence interval. We used Spearman's rank correlation coefficient because it does not assume a linear correlation.

Figure 7 summarizes the results of the correlation analysis of WaterGAP3 data after binning by mean temperature and precipitation. The colors in the plots show correlations between topography and mean runoff (top row) and correlations between topography and snowmelt fraction (bottom row). Green values indicate strong positive correlations, magenta values indicate strong negative correlations, black values indicate weak to no correlation, and gray values indicate that there were not enough observations in the data set to evaluate the correlation. The patterns in correlation are somewhat difficult to interpret as clusters of strong positive correlation are often adjacent to clusters of strong anti-correlation. Topographic predictors of mean runoff show little sensible pattern (Figures 7a–7c), with a hint of positive correlation between local relief and mean runoff at low values of mean precipitation (Figure 7c). Topographic predictors of snowmelt fraction are also complex with a band of positive correlation for lower mean temperatures next to a band of anti-correlation at higher temperatures (Figures 7d–7f). While we hesitate to interpret these subtle patterns, the snowmelt fraction results do suggest that increasing topographic elevation and relief only leads to more snowmelt where temperatures are conducive to it, though why this relation has a slope is not obvious.

As we discuss in more depth in the discussion below, the results from the global analysis suggest that there is no single set of globally applicable “rules” that relate topography to mean runoff and snowmelt fraction. We suspect this is a consequence of the scale of the analysis (i.e., orographic effects are inherently regional) and the lack of accounting for the predominant direction of weather systems with respect to topography (i.e., steep topography is not distinguished as windward vs. leeward). Based on this, we next explore a set of three regional analyses that show more promise in constraining orographic controls on mean runoff and snowmelt fraction.

#### 5.4. Regional Relationships of Mean Runoff and Daily Runoff Variability

Given the challenge of identifying simple relationships between topography (i.e., mean elevation, maximum elevation, and mean local relief) and either mean runoff or snowmelt fraction (Figures 6 and 7), we now examine whether regional relationships between these variables are being obscured by the global treatment. Of the six relationships shown in Figure 7, the relationship between local relief and mean runoff and the relationship between maximum elevation and snowmelt fraction seemed the most promising when evaluated spatially.



**Figure 8.** Relationships among topography, mean runoff, and snowmelt fraction in map view. (a) Mean spearman rank correlation coefficient within a  $2^{\circ}$  moving window for mean runoff and local relief. (b) Mean spearman rank correlation coefficient within a  $2^{\circ}$  moving window for maximum elevation and snowmelt fraction. After filtering the WaterGAP3 data for mountain settings (see text for details), only a small area remains. Insets highlight results for the three regional cases considered.

Figure 8 summarizes the sign and strength of these relationships for all WaterGAP3 data that meet our selection criteria. The zoom insets highlight three regions of interest—namely the mid-latitude mountains of British Columbia, the European Alps, and the Greater Caucasus. Each of these mountain ranges receives a large fraction of its precipitation as snow, with some alpine glaciation under modern climate. In these settings (and others), there is a relatively strong correlation between local relief and mean runoff across the study area (Figure 8a-insets), consistent with prior studies (Bookhagen & Burbank, 2006; Bookhagen & Strecker, 2008). The relationship between maximum elevation and snowmelt fraction is more nuanced (Figure 8b-insets). The sign of the correlation depends on whether positioned on the windward or leeward side of prevailing weather systems, whereby windward sides show relatively strong positive correlations. Nevertheless, the most complex of these three regional sites is the Greater Caucasus, where relationships among maximum elevation, snowmelt fraction, and runoff generation have been verified using a finer-scale analysis of gauge records and hydroclimatic data (Forte et al., 2022). Taken together, this gives us confidence that these three locations are prime candidates for building regional relationships among topography, snowmelt, and runoff statistics. To develop these local relationships, we consider similar candidate relationships tested on the global scale (Figure 7), specifically mean runoff or snowmelt fraction as a function of either mean elevation, maximum elevation, or local relief (Figure S2 in Supporting Information S1).

## 6. Discussion

### 6.1. Mean Runoff, Runoff Variability, and Snowmelt

The global analysis of WaterGAP3 data helped solidify interpretations that mean runoff and daily runoff variability are inversely correlated. This result was born out both in the RFR (Figure 6) and in the individual regressions after binning by snowmelt fraction (Figures 4 and 5), thereby supporting findings from prior studies (Molnar et al., 2006; Rossi et al., 2016). The functional form of the relationship between mean runoff and the shape of the daily runoff distribution appears to bifurcate at snowmelt fractions around 0.35 (Figure 5). Below this value, the relationship is highly nonlinear. Above this value, relationships vary but become much more linear. The nonlinearity in rainfall-runoff regimes can be interpreted using ecohydrological models where climatic parameters can exert different relative influences on mean and tail behavior (Deal et al., 2018). The transition to snowmelt hydrology resulting in lower variability flows (e.g., Pitlick, 1994) is expected due to the effects of both increased runoff ratios and the slow release of water from storage. That abrupt transition emphasizes the importance of the phase transition from rain to snow in event-scale runoff variability. The snowmelt fractions where this occurs are relatively low, suggesting that snowmelt should not be ignored in fluvial erosion models. We also note here that stochastic-threshold models based on stream power were originally developed for small watersheds (e.g., Lague et al., 2005; Tucker, 2004). Given our focus on mountain range scales, it is also important to understand how the spatial footprint of runoff events varies for different runoff generation mechanisms.

To assess the importance of spatial scale to runoff generation, Figure 9 compares the exceedance frequency of the spatial footprints of precipitation and runoff events in the WaterGAP3 data. The area of each “event” is determined by finding spatially contiguous objects in the daily data above a given intensity threshold (i.e., 5–35 mm/day). It should be noted that unlike much of the analysis in previous sections, we do not filter by “mountainous topography” (i.e., use elevation or relief to filter the data), and are considering events across all land surfaces. To convert the unprojected pixel-based objects into areas, we multiplied the number of pixels by the size of a pixel in degrees squared. We then calculated the radius of the circle that equals that area. The radius of the circle is converted from degrees to km in both latitude and longitude. Because the conversion in longitude generally differs from the conversion in latitude, this transformation produces an ellipse with area units of  $\text{km}^2$ . These are the  $x$ -coordinates used for plotting the exceedance frequencies (Figures 9a, 9c, 9e, and 9g). Furthermore, for runoff data, we labeled each event as snowmelt or rainfall runoff based on the 0.35 snowmelt fraction threshold. Because smaller footprints include both rainfall and snowmelt dominated runoff, the right hand panels (Figures 9b, 9d, 9f, and 9h) show the percentage of daily runoff events that are classified as snowmelt for log distributed bins of exceedance frequency. Three important insights emerge from this analysis. First, and unsurprisingly, higher intensity thresholds produce smaller event areas. Second, at around the 25 mm/day threshold, the largest area events in runoff and precipitation (i.e., far right tails) are of similar magnitude. Higher thresholds produce runoff areas larger than comparable frequency precipitation events. Third, the far right tail of the size distribution of runoff is all snowmelt. Taken together, these results suggest that the relative contribution of snowmelt runoff becomes increasingly important for larger watersheds and for increasing intensities.

### 6.2. Importance of Constraining Regional Relationships

While global relationships linking mean runoff and daily runoff variability via topography were elusive, regional assessment was much more promising. Figure 10 summarizes the kinds of regional rulesets that can be generated from an analysis like ours. At the regional scale, relationships between local relief and mean runoff emerge, consistent with other studies focused on explaining spatial patterns in rainfall (e.g., Bookhagen & Burbank, 2006; Bookhagen & Strecker, 2008). This is thought to arise because high relief corresponds to increased forced lifting of air masses. Local relief (not shown) and maximum elevation (shown) also correlate with snowmelt fraction, likely due to the role of high topography increasing the probability that precipitation will fall in the form of snow. Regardless of the mechanisms, our analysis shows the value of producing regionally constrained links between mean runoff and snowmelt fraction via topography. To generate Figure 10, the pixel-based correlation coefficients presented earlier (Figure 8) are summarized into bins of either mean runoff or snowmelt fraction (y-axes). For each bin, the mean and standard deviation of the correlated topographic metric are shown (local relief for mean runoff and maximum elevation for snowmelt fraction). Marker sizes are scaled to the number of observations within a bin. Power law fits for each relationship are shown as lines. In detail, we tested whether better correlations existed between the hydroclimatic variables of interest (mean runoff and snowmelt fraction)

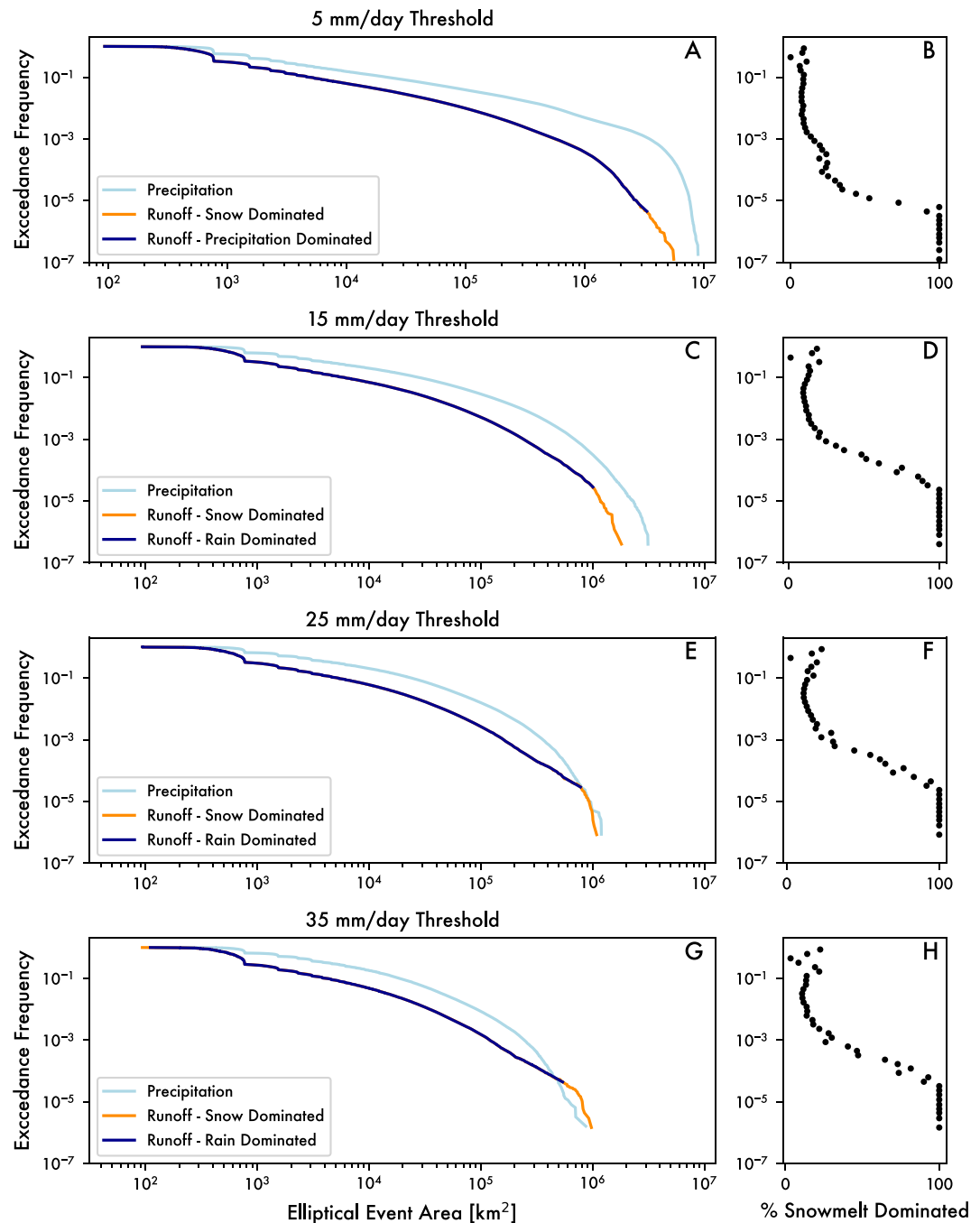


**Figure 9.** Exceedance probability distributions of daily event sizes of different magnitudes: (a and b) 5 mm/day, (c and d) 15 mm/day, (e and f) 25 mm/day, and (g and h) 35 mm/day. The left panels show probability plots for both precipitation and runoff, whereby the latter is color-coded by runoff generation source. After classifying runoff events in this way, the right panels show what fraction of events are snowmelt dominated within the exceedance probability bins. Note that regardless of the intensity threshold the largest area runoff events are snowmelt dominated. At higher intensity thresholds, these event sizes can exceed the largest area precipitation events.

and either mean elevation, maximum elevation, and mean local relief (Figure S2 in Supporting Information S1). The selected relationships shown in Figure 10, that we also use to parameterize the models in Part 2 (Forte & Rossi, 2024a), were chosen primarily based on either goodness of fit (i.e., which relationships had the lowest root mean squared error) or which ones would be more practical to implement in the models developed in Part 2 (Forte & Rossi, 2024a) when the goodness of fit metrics were similar. Each region is described by its own functional

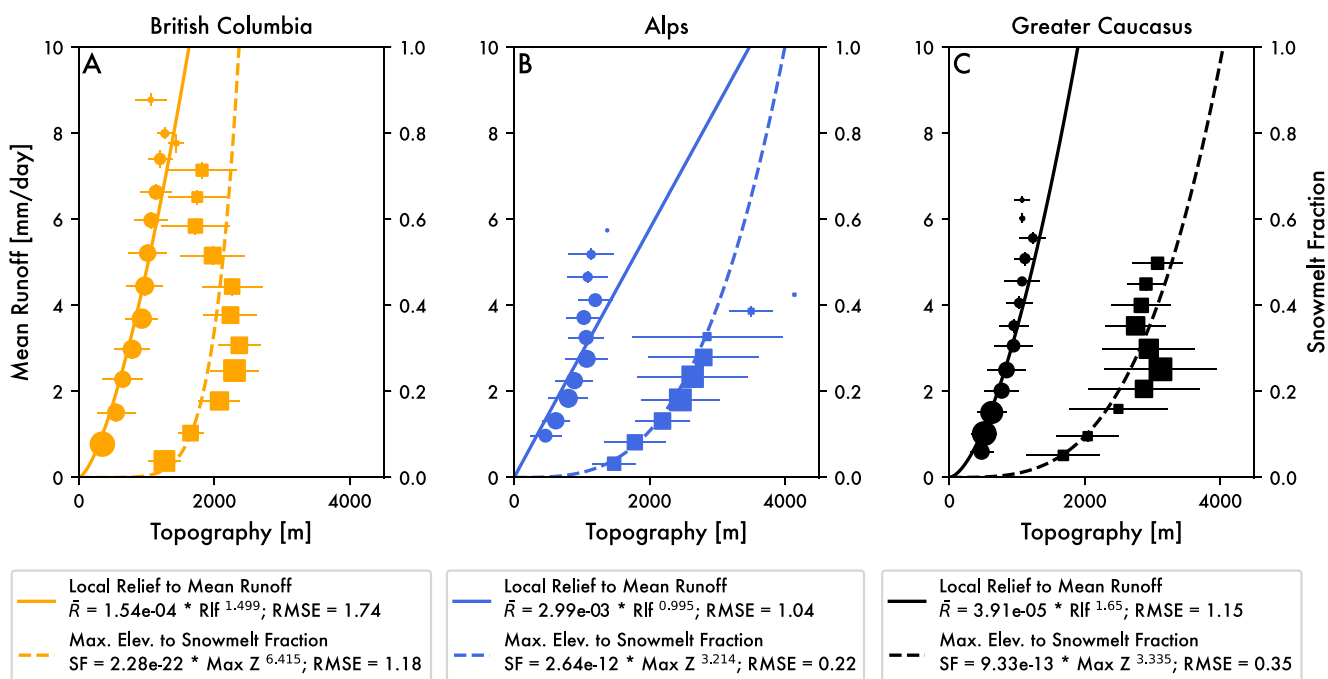


**Figure 10.** Relationships among topography, mean runoff, and snowmelt fraction for the three regional cases (see Figure 8 for locations): (a) British Columbia, (b) European Alps, and (c) Greater Caucasus. In all three plots, circles are binned mean runoff to local relief, and squares are binned snowmelt fraction to maximum elevation. Symbols are scaled to the number of observations in the bin and whiskers show one standard deviation. Power law fits for binned data relate local relief and mean runoff (solid line) and maximum elevation and snowmelt fraction (dashed line). In all three panels, the “Topography” x-axis plots both local relief (solid line) and maximum elevation (dashed line). These fits serve as the basis for orographic rules used in our complementary model study (Forte & Rossi, 2024a).

relationship, which we interpret as the orographic effects on mean runoff and snowmelt fraction for each mountain range. We suspect that some of the non-monotonic behavior of binned values, especially in the snowmelt fraction, is a consequence of mixing windward and leeward components of a regional orographic effect (e.g., Figure 8), as well as along-strike complexity in precipitation sourcing. Nevertheless, summarizing the data in this way allows us to build empirically based rules for mean runoff and snowmelt fraction specific to each region. Together with the observation that the relationship between mean runoff and daily runoff variability abruptly shifts around snowmelt fractions of 0.35 allows us to drive a stochastic runoff model using regionally informed parameters from WaterGAP3 in Part 2 of this analysis (Forte & Rossi, 2024a).

The relationships shown in Figure 10 help explain why the role of topography was so difficult to extract from the RFR that included these metrics (Figure 6). First, regional relationships relating topography to runoff generation are quite noisy. While casting runoff parameters as a simple function of topography was our goal, the relatively coarse resolution of water model data, the lack of distinguishing between windward and leeward slopes, and hydroclimatic diversity induced by regional climate will each confound simple relationships between topography and runoff parameters. Second, while the power law functions decently describe the snowmelt fraction, the bin-averaged values suggest subtle, non-monotonic relationships with maximum elevation. Third, and perhaps most importantly, the relationship for each regional setting is distinctly different. Any global analysis would struggle to parse this difference.

### 6.3. Implications on Landscape Evolution Studies

Two-way coupled models between climate and tectonics require erosion laws for either river incision, glacial erosion, or both. Those testing fluvial dynamics are typically built on the stream power model (e.g., Beaumont et al., 1992; Stolar et al., 2006; Whipple & Meade, 2004; Willett, 1999). Orographic effects in these models focus on the windward ascent and extraction of precipitation. By setting up a contrast in the efficiency of erosion on the windward and leeward sides of mountain ranges, mountain belts adjust their width and height in order to achieve a steady state morphology. The widespread use of stream power in these climate-tectonic models has

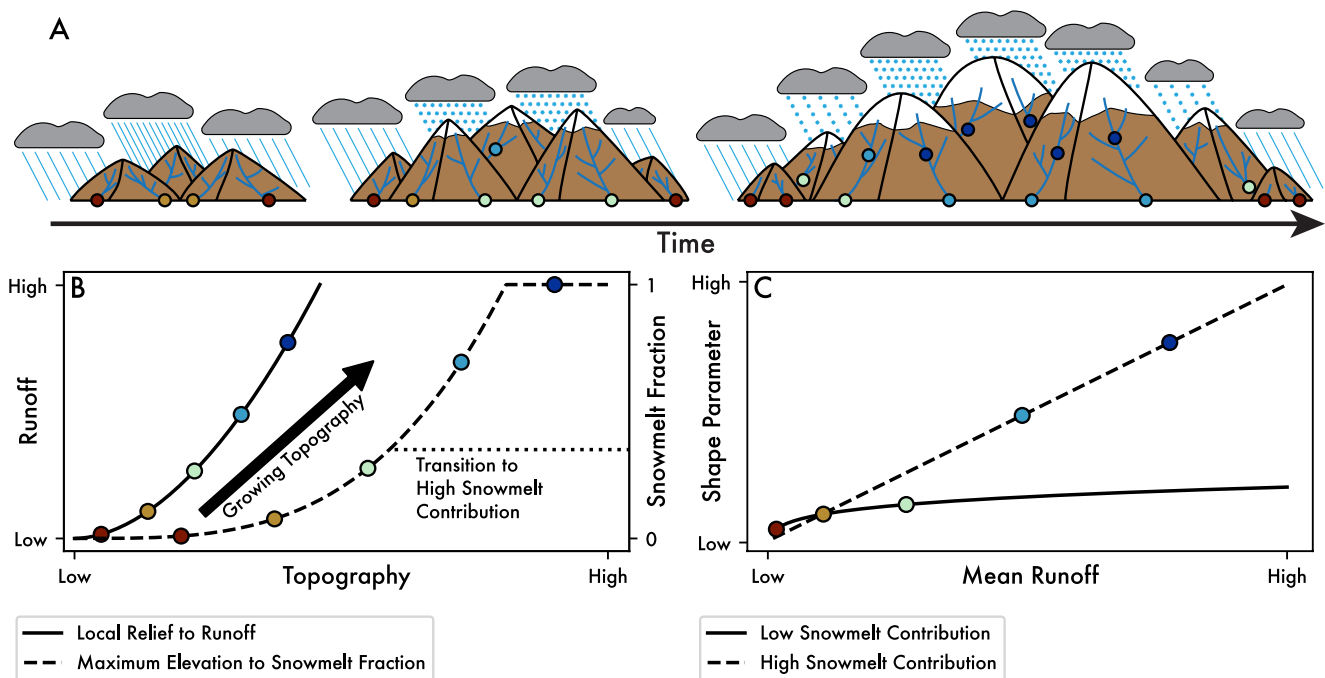


**Figure 11.** A conceptual model for how orographic controls on runoff variability can be represented in a landscape evolution model. (a) Cartoon showing how precipitation and runoff generation mechanisms might change as a mountain range grows. (b) Example rules for how topography is translated into more runoff and a larger snowmelt fraction as topography grows. (c) Relationship between mean runoff and daily runoff variability in response to those rules. In panel (b), the example ruleset shows that as mountain topography grows, increasing relief leads to more runoff generation on the windward side of a mountain range and increasing elevations lead to a higher fraction of snowmelt. In panel (c), these topography-runoff relationships translate into a much different relationship between mean runoff and daily runoff variability that encodes the transition from rainfall- to snowmelt-dominated runoff events.

subsequently motivated many studies to interrogate how orographically induced spatial patterns in precipitation might alter the long-term evolution of river profiles and relief (Anders et al., 2008; Han et al., 2014; Leonard & Whipple, 2021; Roe et al., 2002, 2003). At the same time, stream power models are increasingly incorporating the role of stochastic streamflow and erosion thresholds to interpret river profiles (DiBiase & Whipple, 2011; Lague, 2014; Lague et al., 2005; Marder & Gallen, 2023; Scherler et al., 2017; Snyder et al., 2003; Tucker, 2004; Tucker & Bras, 2000). The aim of this study was to integrate these two productive research threads and explore whether mean runoff, daily runoff variability, and snowmelt fraction can be linked to each other via topographic elevation and relief. As such, we focused our regional analyses on mid-latitude mountain ranges at or near the cusp of glaciation, and where snowmelt contributions to streamflow are significant. While this was our focus, it is worth noting that orographic gradients in stochastic rainfall itself are often poorly constrained. For example, in tropical settings, there can be complex interactions among rainfall types (e.g., convective, monsoonal) that can lead to lower elevation peaks in rainfall maxima (Anders & Nesbitt, 2015) than conventional orographic rules assume, a topic in need of more attention.

Figure 11 is a conceptual diagram illustrating how stochastic runoff parameters might co-evolve with mountain topography in settings where mountain range relief is sufficient to trigger the transition from rainfall-dominated to snowmelt-influence runoff but where river incision is still setting the relief structure of the landscape (e.g., Whipple et al., 1999). The color coded dots on the schematic mountains in Figure 11a are intended to correspond to the dots on the hypothetical plots relating topography to runoff and snowmelt (Figure 11b) and those relating mean runoff to daily runoff variability (Figure 11c). On the windward side of mountain ranges, we expect that the growth of topography will increase mean runoff (Figure 11b solid line) in line with conventional treatments of orographic precipitation (Roe, 2005). This leads to concurrent increases in the frequency of snowfall and thus the snowmelt contribution to runoff (Figure 11b dashed line). While the snowmelt fraction has an upper bound of one, in practice, the upper bound we are envisioning in Figure 11b will be less than one because rain continues to fall at lower elevations and because the temperatures required to enhance very high snowmelt fractions would also entail a transition to glaciation. The key behavior in this conceptual framework is that accounting for snowmelt dynamics leads to a markedly different relationship between mean runoff and

the shape parameter of the daily runoff distribution (Figure 11c). Our global analysis of WaterGAP3 data suggests that this transition might be abrupt. We identified a snowmelt fraction of  $\sim 0.35$  corresponds to this transition, with the important caveat that this is based on a water model data set that tends to produce underestimates of the shape parameter (Figure 3b). Furthermore, while the bulk of the data supports the notion that this transition is relatively abrupt, there are a number of exceptions to this pattern in both the water model and observational data (Figures 1b, 4, and 5a). These exceptions may be due to uncertainty in the proposed snowmelt transition or evidence for the numerous other hydrological considerations that can reduce daily variability in rainfall-dominated regimes (e.g., seasonality, groundwater, drainage basin size). Regardless, the global analysis reveals that the strength and form of these relationships need to be assessed independently for any given mountain range (Figure 10). However, by simplifying the hydrology into just two parameters, these kinds of relationships are well-suited to driving long-term models of river incision (e.g., Lague et al., 2005; Tucker, 2004) in ways that can be linked to mean climate (DiBiase & Whipple, 2011) and ecohydrology (Deal et al., 2018).

While we think there is observational evidence for these dynamics in actual landscapes (Forte et al., 2022), we highlight a few important caveats to generalizing from our large-scale analysis of the WaterGAP3 water model data. First, this conceptual model is better suited to explaining the windward side of mountain ranges where precipitation, and thus runoff, is enhanced by topography. To build better rulesets, higher resolution runoff data sets that honor physiographic transitions and water divides are likely needed. Second, this conceptual model requires that mean runoff and rare runoff events are linked via some common mechanism. This need not be the case. For example, recent work in the Colorado Front Range showed how mean runoff was largely driven by snowmelt throughout the landscape while daily runoff variability was driven by rainfall runoff at lower elevations in response to thinning soils (Rossi et al., 2020). Such mechanistic controls on mean runoff and daily runoff variability are at play in all landscapes and may partially explain the wide variance of runoff parameters observed in our regional rulesets (Figure 10). Third, statistical analyses all assumed independence of daily runoff events, which is decidedly not true as runoff events, especially large ones, can extend over multiple days (synoptic-scale storms) to seasons (snowmelt, monsoons). Despite these caveats, this analysis produced empirically-based runoff parameters that vary in space and time. As such, this provides the minimal constraints needed to integrate orographic effects with stochastic runoff generation for river profile modeling (Forte & Rossi, 2024a).

## 7. Conclusions

The results of our global analysis of WaterGAP3 data largely confirm, and significantly expand upon, past results indicating a negative correlation between mean runoff and daily runoff variability. The form of the relationship between variability and mean runoff is linked to the fraction of runoff from snowmelt. For snowmelt fractions  $<0.35$ , mean runoff and variability are related by a power law. At higher snowmelt fractions, the two are linearly related. We also find that snowmelt produces runoff events with a much larger areal extent than rainfall runoff.

Exploration of the extent to which mean runoff, runoff variability, and snowmelt fraction are related to topography produces ambiguous results at the global scale. Unsupervised machine learning methods highlight that simple topographic variables such as mean elevation, maximum elevation, and local relief do not have strong predictive power for our target hydroclimatological parameters of mean runoff, snowmelt fraction, and daily runoff variability. Attempts to identify cross-correlations that may mask the role of topography were more suggestive but still difficult to interpret. Results from the global analysis emphasize that exploring the relationships between topography and hydroclimatology requires a regional approach. For three mid-latitude mountain ranges – the European Alps, Greater Caucasus, and southern British Columbia—we found robust positive relationships between mean runoff and mean local relief and snowmelt fraction and maximum elevation.

The links between topography, mean runoff, daily runoff variability, and snowmelt fraction highlight that multiple aspects of the hydroclimate of mountain ranges should be expected to evolve as topography grows. Past work on this topic has primarily focused on the influence of growing topography on the development of orographic patterns in rainfall. When coupled to tectonic models and simple hydrologic models equating patterns in mean rainfall to mean runoff, orographic effects have been shown to drive a variety of feedback between surface processes and tectonics. Our results show how to move beyond mean precipitation or mean runoff when considering the coupled evolution of topography, tectonics, and climate. Both snowmelt fraction and mean runoff are expected to increase with growing topography and reduce daily runoff variability, emphasizing the need to explicitly consider snowmelt dynamics in coupled tectonic–landscape evolution models.

## Data Availability Statement

Analysis codes necessary to reproduce this work are available in Forte (2024). Larger outputs of the processing steps are available in Forte and Rossi (2024b). Portions of these analysis codes rely on publicly available data sets that we do not have the permission to redistribute, but when used, we provide comments in the code referencing where these data sets can be downloaded.

## Acknowledgments

Support for M.W. Rossi came from the NSF Geomorphology and Land-use Dynamics (GLD) Program (EAR-1822062). Neither AMF nor MWR have any real or perceived financial or other conflicts with the contents of this work. We thank Mikael Attal for editorial handling and also Associate Editor Liran Goren and reviewers Alison Anders, Eric Deal, and an anonymous reviewer for their comments that improved this manuscript.

## References

Adam, J. C., Hamlet, A. F., & Lettenmaier, D. P. (2009). Implications of global climate change for snowmelt hydrology in the twenty-first century. *Hydrological Processes*, 23(7), 962–972. <https://doi.org/10.1002/hyp.7201>

Adams, B. A., Whipple, K. X., Forte, A. M., Heimsath, A. M., & Hodges, K. V. (2020). Climate controls on erosion in tectonically active landscapes. *Science Advances*, 6(42). <https://doi.org/10.1126/sciadv.aaz3166>

Alcamo, J., Döll, P., Henrichs, T., Kaspar, F., Lehner, B., Rösch, T., & Siebert, S. (2003). Development and testing of the WaterGAP 2 global model of water use and availability. *Hydrological Sciences Journal*, 48(3), 317–337. <https://doi.org/10.1623/hysj.48.3.317.45290>

Anders, A. M., & Nesbitt, S. W. (2015). Altitudinal precipitation gradients in the Tropics from tropical rainfall measuring mission (TRMM) precipitation radar. *Journal of Hydrometeorology*, 16(1), 441–448. <https://doi.org/10.1175/JHM-D-14-0178.1>

Anders, A. M., Roe, G. H., Montgomery, D. R., & Hallet, B. (2008). Influence of precipitation phase on the form of mountain ranges. *Geology*, 36(6), 479. <https://doi.org/10.1130/G24821A.1>

Barnett, T. P., Adam, J. C., & Lettenmaier, D. P. (2005). Potential impacts of a warming climate on water availability in snow-dominated regions. *Nature*, 438(7066), 303–309. <https://doi.org/10.1038/nature04141>

Barnhart, T. B., Molotch, N. P., Livneh, B., Harpold, A. A., Knowles, J. F., & Schneider, D. (2016). Snowmelt rate dictates streamflow. *Geophysical Research Letters*, 43(15), 8006–8016. <https://doi.org/10.1002/2016GL069690>

Barros, A. P., & Lettenmaier, D. P. (1994). Dynamic modeling of orographically induced precipitation. *Reviews of Geophysics*, 32(3), 265–284. <https://doi.org/10.1029/94RG00625>

Basso, S., Merz, R., Tarasova, L., & Minissi, A. (2023). Extreme flooding controlled by stream network organization and flow regime. *Nature Geoscience*, 16(4), 339–343. <https://doi.org/10.1038/s41561-023-01155-w>

Beaumont, C., Fullsack, P., & Hamilton, J. (1992). Erosional control of active compressional orogens. In K. R. McClay (Ed.), *Thrust tectonics* (pp. 1–18). Chapman Hall.

Beck, H. E., van Dijk, A. I. J. M., de Roo, A., Dutra, E., Fink, G., Orth, R., & Schellekens, J. (2017). Global evaluation of runoff from 10 state-of-the-art hydrological models. *Hydrology and Earth System Sciences*, 21(6), 2881–2903. <https://doi.org/10.5194/hess-21-2881-2017>

Berghuijs, W. R., Harrigan, S., Molnar, P., Slater, L. J., & Kirchner, J. W. (2019). The relative importance of different flood-generating mechanisms across Europe. *Water Resources Research*, 55(6), 4582–4593. <https://doi.org/10.1029/2019WR024841>

Berghuijs, W. R., Woods, R. A., & Hrachowitz, M. (2014). A precipitation shift from snow towards rain leads to a decrease in streamflow. *Nature Climate Change*, 4(7), 583–586. <https://doi.org/10.1038/nclimate2246>

Bookhagen, B., & Burbank, D. (2006). Topography, relief, and TRMM-derived rainfall variations along the Himalaya. *Geophysical Research Letters*, 33(8), L08405. <https://doi.org/10.1029/2006GL026037>

Bookhagen, B., & Burbank, D. (2010). Toward a complete Himalayan hydrological budget: Spatiotemporal distribution of snowmelt and rainfall and their impact on river discharge. *Journal of Geophysical Research*, 115(F3), F03019. <https://doi.org/10.1029/2009JF001426>

Bookhagen, B., & Strecker, M. R. (2008). Orographic barriers, high-resolution TRMM rainfall, and relief variations in the eastern Andes. *Geophysical Research Letters*, 35(6), L06403. <https://doi.org/10.1029/2007GL032011>

Bookhagen, B., & Strecker, M. R. (2011). Modern Andean rainfall variation during ENSO cycles and its impact on the Amazon Drainage Basin. In C. Hoorn & F. P. Wesseling (Eds.), *Amazonia: Landscape and Species Evolution* (pp. 223–241). Wiley-Blackwell Publishing Ltd. <https://doi.org/10.1002/9781444306408.ch14>

Botter, G., Porporato, A., Rodriguez-Iturbe, I., & Rinaldo, A. (2009). Nonlinear storage-discharge relations and catchment streamflow regimes. *Water Resources Research*, 45(10), W10427. <https://doi.org/10.1029/2008WR007658>

Campforts, B., Vanacker, V., Herman, F., Vanmaercke, M., Schwanghart, W., Tenorio, G. E., et al. (2020). Parameterization of river incision models requires accounting for environmental heterogeneity: Insights from the tropical Andes. *Earth Surface Dynamics*, 8(2), 447–470. <https://doi.org/10.5194/esurf-8-447-2020>

Crave, A., & Davy, P. (2001). A stochastic “precipiton” model for simulating erosion/sedimentation dynamics. *Computers & Geosciences*, 27(7), 815–827. [https://doi.org/10.1016/S0098-3004\(00\)00167-9](https://doi.org/10.1016/S0098-3004(00)00167-9)

Deal, E., Braun, J., & Botter, G. (2018). Understanding the role of rainfall and hydrology in determining fluvial erosion efficiency. *Journal of Geophysical Research: Earth Surface*, 123(4), 744–778. <https://doi.org/10.1029/2017JF004393>

Deal, E., Favre, A. C., & Braun, J. (2017). Rainfall variability in the Himalayan orogen and its relevance to erosion processes. *Water Resources Research*, 53(5), 4004–4021. <https://doi.org/10.1002/2016WR020030>

Decharme, B., Alkama, R., Douville, H., Becker, M., & Cazenave, A. (2010). Global evaluation of the ISBA-TRIP continental hydrological system. Part II: Uncertainties in river routing simulation related to flow velocity and groundwater storage. *Journal of Hydrometeorology*, 11(3), 601–617. <https://doi.org/10.1175/2010JHM1212.1>

Decharme, B., Martin, E., & Faroux, S. (2013). Reconciling soil thermal and hydrological lower boundary conditions in land surface models. *Journal of Geophysical Research: Atmospheres*, 118(14), 7819–7834. <https://doi.org/10.1029/jgrd.50631>

Desormeaux, C., Godard, V., Lague, D., Duclaux, G., Fleury, J., Benedetti, L., & Bellier, O. (2022). Investigation of stochastic-threshold incision models across a climatic and morphological gradient. *Earth Surface Dynamics*, 10(3), 473–492. <https://doi.org/10.5194/esurf-10-473-2022>

DiBiase, R. A., & Whipple, K. X. (2011). The influence of erosion thresholds and runoff variability on the relationships among topography, climate, and erosion rate. *Journal of Geophysical Research*, 116(F4), F04036. <https://doi.org/10.1029/2011JF002095>

DiBiase, R. A., Whipple, K. X., Heimsath, A. M., & Ouimet, W. B. (2010). Landscape form and millennial erosion rates in the San Gabriel Mountains, CA. *Earth and Planetary Science Letters*, 289(1–2), 134–144. <https://doi.org/10.1016/j.epsl.2009.10.036>

Doane, D. P. (1976). Aesthetic frequency classifications. *The American Statistician*, 30(4), 181–183. <https://doi.org/10.1080/00031305.1976.10479172>

Döll, P., Kaspar, F., & Lehner, B. (2003). A global hydrological model for deriving water availability indicators: Model tuning and validation. *Journal of Hydrology*, 270(1–2), 105–134. [https://doi.org/10.1016/S0022-1694\(02\)00283-4](https://doi.org/10.1016/S0022-1694(02)00283-4)

Dupuis, D. J. (1998). Exceedances over high thresholds: A guide to threshold selection. *Extremes*, 1(3), 251–261. <https://doi.org/10.1023/a:1009914915709>

Eagleson, P. S. (1978). Climate, soil, and vegetation: 2. The distribution of annual precipitation derived from observed storm sequences. *Water Resources Research*, 14(5), 713–721. <https://doi.org/10.1029/WR014i005p00713>

Eisner, S. (2015). *Comprehensive evaluation of the waterGAP3 model across climatic, physiographic, and anthropogenic gradients*. University of Kassel.

Falcone, J. A. (2011). GAGES-II: Geospatial attributes of gages for evaluating streamflow (Report). <https://doi.org/10.3133/70046617>

Farr, T. G., Rosen, P. A., Caro, E., Crippen, R., Duren, R., Hensley, S., et al. (2007). The shuttle radar topography mission. *Reviews of Geophysics*, 45(2), 1–33. <https://doi.org/10.1029/2005rg000183>

Faticchi, S., Vivoni, E. R., Ogden, F. L., Ivanov, V. Y., Mirus, B., Gochis, D., et al. (2016). An overview of current applications, challenges, and future trends in distributed process-based models in hydrology. *Journal of Hydrology*, 537, 45–60. <https://doi.org/10.1016/j.jhydrol.2016.03.026>

Forte, A. M. (2024). amforte/snowmelt Orography: Snowmelt Orography (Version v2.0) [Dataset]. Zenodo. <https://doi.org/10.5281/zenodo.1044937>

Forte, A. M., Leonard, J. S., Rossi, M. W., Whipple, K. X., Heimsath, A. M., Sukhishvili, L., et al. (2022). Low variability runoff inhibits coupling of climate, tectonics, and topography in the Greater Caucasus. *Earth and Planetary Science Letters*, 584, 117525. <https://doi.org/10.1016/j.epsl.2022.117525>

Forte, A. M., & Rossi, M. W. (2024a). Stochastic in space and time: Part 2, effects of simulating orographic gradients in daily runoff variability on bedrock incision. *Journal of Geophysical Research: Earth Surface*. <https://doi.org/10.1029/2023JF007327>

Forte, A. M., & Rossi, M. W. (2024b). Data and model results associated with stochastic in space and time: Parts 1 and 2. (Version 2.0) [Dataset]. Zenodo. <https://doi.org/10.5281/zenodo.10407347>

Forte, A. M., Whipple, K. X., Bookhagen, B., & Rossi, M. W. (2016). Decoupling of modern shortening rates, climate, and topography in the Caucasus. *Earth and Planetary Science Letters*, 449, 282–294. <https://doi.org/10.1016/j.epsl.2016.06.013>

Galewsky, J. (2009). Rain shadow development during the growth of mountain ranges: An atmospheric dynamics perspective. *Journal of Geophysical Research*, 114(F1), F01018. <https://doi.org/10.1029/2008JF001085>

Grömping, U. (2009). Variable importance assessment in regression: Linear regression versus random forest. *The American Statistician*, 63(4), 308–319. <https://doi.org/10.1198/tast.2009.08199>

Han, J., Gasparini, N. M., Johnson, J. P. L., & Murphy, B. P. (2014). Modeling the influence of rainfall gradients on discharge, bedrock erodibility, and river profile evolution, with application to the Big Island, Hawai'i. *Journal of Geophysical Research*, 119(6), 1418–1440. <https://doi.org/10.1002/203JF002961>

Harel, M. A., Mudd, S. M., & Attal, M. (2016). Global analysis of the stream power law parameters based on worldwide <sup>10</sup>Be denudation rates. *Geomorphology*, 268, 184–196. <https://doi.org/10.1016/j.geomorph.2016.05.035>

Howard, A. D. (1994). A detachment-limited model of drainage basin evolution. *Water Resources Research*, 30(7), 2261–2285. <https://doi.org/10.1029/94wr00757>

Huang, X., & Niemann, J. D. (2006). An evaluation of the geomorphically effective event for fluvial processes over long periods. *Journal of Geophysical Research*, 111(F3), F03015. <https://doi.org/10.1029/2006JF000477>

Jiang, Q. (2003). Moist dynamics and orographic precipitation. *Tellus A: Dynamic Meteorology and Oceanography*, 55(4), 301. <https://doi.org/10.3402/tellusa.v55i4.14577>

Kirby, E., & Whipple, K. X. (2012). Expression of active tectonics in erosional landscapes. *Journal of Structural Geology*, 44, 54–75. <https://doi.org/10.1016/j.jsg.2012.07.009>

Kirchner, J. W. (2009). Catchments as simple dynamical systems: Catchment characterization, rainfall-runoff modeling, and doing hydrology backward. *Water Resources Research*, 45(2), W02429. <https://doi.org/10.1029/2008WR006912>

Lague, D. (2014). The stream power river incision model: Evidence, theory and beyond. *Earth Surface Processes and Landforms*, 39(1), 38–61. <https://doi.org/10.1002/esp.3462>

Lague, D., Hovius, N., & Davy, P. (2005). Discharge, discharge variability, and the bedrock channel profile. *Journal of Geophysical Research*, 110(F4), F04006. <https://doi.org/10.1029/2004JF000259>

Laherrère, J., & Sornette, D. (1998). Stretched exponential distributions in nature and economy: “fat tails” with characteristic scales. *The European Physical Journal B*, 2(4), 525–539. <https://doi.org/10.1007/s100510050276>

Lehner, B., Verdin, K., & Jarvis, A. (2008). New global hydrography derived from spaceborne elevation data. *Eos, Transactions American Geophysical Union*, 89(10), 93–94. <https://doi.org/10.1029/2008EO100001>

Leonard, J. S., & Whipple, K. X. (2021). Influence of spatial rainfall gradients on river longitudinal profiles and the topographic expression of spatially and temporally variable climates in mountain landscapes. *Journal of Geophysical Research: Earth Surface*, 126(12), e2021JF006183. <https://doi.org/10.1029/2021JF006183>

Leonard, J. S., Whipple, K. X., & Heimsath, A. M. (2023). Isolating climatic, tectonic, and lithologic controls on mountain landscape evolution. *Science Advances*, 9(3), eadd8915. <https://doi.org/10.1126/sciadv.add8915>

Lins, H. F. (2012). USGS hydro-climatic data network 2009 (HCDN-2009) (US Geological Survey Fact Sheet 3047 No. 4). Retrieved from <https://pubs.usgs.gov/fs/2012/3047/pdf/fs2012-3047.pdf>

Malamud, B. D., & Turcotte, D. L. (2006). The applicability of power-law frequency statistics to floods. *Journal of Hydrology*, 322(1–4), 168–180. <https://doi.org/10.1016/j.jhydrol.2005.02.032>

Marder, E., & Gallen, S. F. (2023). Climate control on the relationship between erosion rate and fluvial topography. *Geology*, 51(5), 424–427. <https://doi.org/10.1130/G50832.1>

Molnar, P., Anderson, R. S., Kier, G., & Rose, J. (2006). Relationships among probability distributions of stream discharges in floods, climate, bed load transport, and river incision. *Journal of Geophysical Research*, 111(F2), F02001. <https://doi.org/10.1029/2005JF000310>

Nesbitt, S. W., & Anders, A. M. (2009). Very high resolution precipitation climatologies from the Tropical Rainfall Measuring Mission precipitation radar. *Geophysical Research Letters*, 36(15), L15815. <https://doi.org/10.1029/2009GL038026>

Pitlick, J. (1994). Relation between peak flows, precipitation, and physiography for five mountain regions in the western USA. *Journal of Hydrology*, 158(3–4), 219–240. [https://doi.org/10.1016/0022-1694\(94\)90055-8](https://doi.org/10.1016/0022-1694(94)90055-8)

Roe, G. H. (2005). Orographic precipitation. *Annual Review of Earth and Planetary Sciences*, 33(1), 645–671. <https://doi.org/10.1146/annurev.earth.33.092203.122541>

Roe, G. H., Montgomery, D. R., & Hallet, B. (2002). Effects of orographic precipitation variations on the concavity of steady-state river profiles. *Geology*, 30(2), 143–146. [https://doi.org/10.1130/0091-7613\(2002\)030<0143:eoopo>2.0.co;2](https://doi.org/10.1130/0091-7613(2002)030<0143:eoopo>2.0.co;2)

Roe, G. H., Montgomery, D. R., & Hallet, B. (2003). Orographic precipitation and the relief of mountain ranges. *Journal of Geophysical Research*, 108(B6), 2315. <https://doi.org/10.1029/2001JB001521>

Rossi, M. W., Anderson, R. S., Anderson, S. P., & Tucker, G. E. (2020). Orographic controls on subdaily rainfall statistics and flood frequency in the Colorado Front Range, USA. *Geophysical Research Letters*, 47(4), e2019GL085086. <https://doi.org/10.1029/2019GL085086>

Rossi, M. W., Whipple, K. X., & Vivoni, E. R. (2016). Precipitation and evapotranspiration controls on event-scale runoff variability in the contiguous United States and Puerto Rico. *Journal of Geophysical Research*, 121(1), 128–145. <https://doi.org/10.1002/2015JF003446>

Schaefli, B., Rinaldo, A., & Botter, G. (2013). Analytic probability distributions for snow-dominated streamflow. *Water Resources Research*, 49(5), 2701–2713. <https://doi.org/10.1002/wrcr.20234>

Schellekens, J., Dutra, E., Weiland, F. S., Minvielle, M., Calvet, J.-C., Decharme, B., et al. (2017). A global water resources ensemble of hydrological models: The earth2Observe Tier-1 dataset. *Earth System Data Science*, 9(2), 389–413. <https://doi.org/10.5194/essd-9-389-2017>

Scherler, D., DiBiase, R. A., Fisher, G. B., & Avouac, J.-P. (2017). Testing monsoonal controls on bedrock river incision in the Himalaya and Eastern Tibet with a stochastic-threshold stream power model. *Journal of Geophysical Research: Earth Surface*, 122(7), 1389–1429. <https://doi.org/10.1002/2016JF004011>

Schmid, H., Cáceres, D., Eisner, S., Flörke, M., Herbert, C., Niemann, C., et al. (2020). The global water resources and use model WaterGAP v2.2d: Model description and evaluation. *Geoscientific Model Development*, 14, 1037–1079. <https://doi.org/10.5194/gmd-2020-225>

Schmid, H., Eisner, S., Franz, D., Wattenbach, M., Portmann, F. T., Flörke, M., & Döll, P. (2014). Sensitivity of simulated global-scale freshwater fluxes and storages to input data, hydrological model structure, human water use and calibration. *Hydrology and Earth System Sciences*, 18(9), 3511–3538. <https://doi.org/10.5194/hess-18-3511-2014>

Schwanghart, W., & Scherler, D. (2014). Short Communication: TopoToolbox 2 - MATLAB based software for topographic analysis and modeling in earth surface sciences. *Earth Surface Dynamics*, 2, 1–7. <https://doi.org/10.5194/esurf-2-1-2014>

Shen, H., Lynch, B., Poulsen, C. J., & Yanites, B. J. (2021). A modeling framework (WRF-Landlab) for simulating orogen-scale climate-erosion coupling. *Computers & Geosciences*, 146, 104625. <https://doi.org/10.1016/j.cageo.2020.104625>

Shobe, C. M., Tucker, G. E., & Anderson, R. S. (2016). Hillslope-derived blocks retard river incision. *Geophysical Research Letters*, 43(10), 5070–5078. <https://doi.org/10.1002/2016GL069262>

Sivapalan, M., Jothityangkoon, C., & Menabde, M. (2002). Linearity and nonlinearity of basin response as a function of scale: Discussion of alternative definitions. *Water Resources Research*, 38(2), 4–1–4–5. <https://doi.org/10.1029/2001WR000482>

Smith, R. B. (1979). The influence of mountains on the atmosphere. In B. Saltzman (Ed.), *Advances in Geophysics* (Vol. 21, pp. 87–230). Elsevier. [https://doi.org/10.1016/S0065-2687\(08\)60262-9](https://doi.org/10.1016/S0065-2687(08)60262-9)

Smith, R. B., & Barstad, I. (2004). A linear theory of orographic precipitation. *Journal of the Atmospheric Sciences*, 61(12), 1377–1391. [https://doi.org/10.1175/1520-0469\(2004\)061<1377:ALTOOP>2.0.CO;2](https://doi.org/10.1175/1520-0469(2004)061<1377:ALTOOP>2.0.CO;2)

Snyder, N. P., Whipple, K. X., Tucker, G. E., & Merritts, D. J. (2003). Importance of a stochastic distribution of floods and erosion thresholds in the bedrock river incision problem. *Journal of Geophysical Research*, 108(B2), 2117. <https://doi.org/10.1029/2001JB001655>

Stolar, D. B., Willett, S. D., & Roe, G. H. (2006). Climatic and tectonic forcing of a critical orogen. In S. D. Willett, N. Hovius, M. T. Brandon, & D. Fisher (Eds.), *Tectonics, climate, and landscape evolution* (Vol. 398, pp. 241–250). Geological Society of America.

Trenberth, K. E., Dai, A., Rasmusson, R. M., & Parsons, D. B. (2003). The changing character of precipitation. *Bulletin of the American Meteorological Society*, 84(9), 1205–1218. <https://doi.org/10.1175/BAMS-84-9-1205>

Tucker, G. E. (2004). Drainage basin sensitivity to tectonic and climatic forcing: Implications of a stochastic model for the role of entrainment and erosion thresholds. *Earth Surface Processes and Landforms*, 29(2), 185–204. <https://doi.org/10.1002/esp.1020>

Tucker, G. E., & Bras, R. L. (2000). A stochastic approach to modeling the role of rainfall variability in drainage basin evolution. *Water Resources Research*, 36(7), 1953–1964. <https://doi.org/10.1029/2000wr900065>

Walter, M. T., Brooks, E. S., McCool, D. K., King, L. G., Molnau, M., & Boll, J. (2005). Process-based snowmelt modeling: Does it require more input data than temperature-index modeling? *Journal of Hydrology*, 300(1–4), 65–75. <https://doi.org/10.1016/j.jhydrol.2004.05.002>

Whipple, K. X. (2009). Landscape texture set to scale. *Nature*, 460(7254), 468–469. <https://doi.org/10.1038/460468a>

Whipple, K. X., DiBiase, R. A., Crosby, B., & Johnson, J. P. L. (2022). Bedrock rivers. In J. Jack & F. Shroder (Eds.), *Treatise on Geomorphology* (2nd ed., pp. 865–903). Academic Press. <https://doi.org/10.1016/B978-0-12-818234-5.00101-2>

Whipple, K. X., Hancock, G. S., & Anderson, R. S. (2000). River incision into bedrock: Mechanics and relative efficacy of plucking, abrasion, and cavitation. *Geology*, 112(3), 490–503. [https://doi.org/10.1130/0016-7606\(2000\)112<490:riibma>2.0.co;2](https://doi.org/10.1130/0016-7606(2000)112<490:riibma>2.0.co;2)

Whipple, K. X., Kirby, E., & Brocklehurst, S. H. (1999). Geomorphic limits to climate-induced increases in topographic relief. *Nature*, 401(6748), 39–43. <https://doi.org/10.1038/43375>

Whipple, K. X., & Meade, B. (2004). Controls on the strength of coupling among climate, erosion, and deformation in two-sided, frictional orogenic wedges at steady state. *Journal of Geophysical Research*, 109(F1), F01011. <https://doi.org/10.1029/2003JF000019>

Whipple, K. X., & Tucker, G. E. (1999). Dynamics of the stream-power river incision model: Implications for height limits of mountain ranges, landscape response timescales, and research needs. *Journal of Geophysical Research*, 104(B8), 17661–17674. <https://doi.org/10.1029/1999jb900120>

Whittaker, A. C. (2012). How do landscapes record tectonics and climate. *Lithosphere*, 4(2), 160–164. <https://doi.org/10.1130/rf.1003.1>

Willett, S. D. (1999). Orogeny and orography: The effects of erosion on the structure of mountain belts. *Journal of Geophysical Research*, 104(B12), 28957–28981. <https://doi.org/10.1029/1999jb900248>

Wilson, P. S., & Toumi, R. (2005). A fundamental probability distribution for heavy rainfall. *Geophysical Research Letters*, 32(14), L14812. <https://doi.org/10.1029/2005GL022465>

Wobus, C. W., Whipple, K. X., Kirby, E., Snyder, N. P., Johnson, J., Spyropoulou, K., et al. (2006). Tectonics from topography: Procedures, promise, and pitfalls. In S. D. Willett, N. Hovius, M. T. Brandon, & D. Fisher (Eds.), *Tectonics, climate, and landscape evolution* (Vol. 1–398, pp. 55–74). The Geological Society of America.